(12) LEVEL II

(14) DNA 5159F-1

(6)

DELFIC: DEPARTMENT OF DEFENSE FALLOUT PREDICTION SYSTEM

Volume I - Fundamentals

Atmospheric Science Associates
P.O. Box 307
Bedford, Massachusetts 01730

(11) 31 Dec 1979

(12) 91

(1) Final Report for Period 16 Jan 1979—31 Dec 1979

CONTRACT No. DNA 001-76-C-0010

(15)

THIS WORK SPONSORED BY THE DEFENSE NUCLEAR AGENCY
UNDER RDT&E RMSS CODE B325076464 V99QAXNA01102 H2590D.

(16)

(17) H 211

Prepared for
Director
DEFENSE NUCLEAR AGENCY
Washington, D. C. 20305

Destroy this report when it is no longer needed. Do not return to sender.

PLEASE NOTIFY THE DEFENSE NUCLEAR AGENCY, ATTN: TISI, WASHINGTON, D.C. 20305, IF YOUR ADDRESS IS INCORRECT, IF YOU WISH TO BE DELETED FROM THE DISTRIBUTION LIST, OR IF THE ADDRESSEE IS NO LONGER EMPLOYED BY YOUR ORGANIZATION.

UNCLASSIFIED

SECURITY CLASSIFICATION OF THIS PAGE *(When Data Entered)*

REPORT DOCUMENTATION PAGE		READ INSTRUCTIONS BEFORE COMPLETING FORM
1. REPORT NUMBER DNA 5159F-1	2. GOVT ACCESSION NO.	3. RECIPIENT'S CATALOG NUMBER
4. TITLE *(and Subtitle)* DELFIC: DEPARTMENT OF DEFENSE FALLOUT PREDICTION SYSTEM Volume I—Fundamentals		5. TYPE OF REPORT & PERIOD COVERED Final Report for Period 16 Jan 79—31 Dec 79 6. PERFORMING ORG. REPORT NUMBER
7. AUTHOR(s) Hillyer G. Norment		8. CONTRACT OR GRANT NUMBER(s) DNA 001-76-C-0010
9. PERFORMING ORGANIZATION NAME AND ADDRESS Atmospheric Science Associates P.O. Box 307 Bedford, Massachusetts 01730		10. PROGRAM ELEMENT, PROJECT, TASK AREA & WORK UNIT NUMBERS Subtask V99QAXNA011-02
11. CONTROLLING OFFICE NAME AND ADDRESS Director Defense Nuclear Agency Washington, D.C. 20305		12. REPORT DATE 31 December 1979 13. NUMBER OF PAGES 100
14. MONITORING AGENCY NAME & ADDRESS *(if different from Controlling Office)*		15. SECURITY CLASS *(of this report)* UNCLASSIFIED 15a. DECLASSIFICATION/DOWNGRADING SCHEDULE

16. DISTRIBUTION STATEMENT *(of this Report)*

Approved for public release; distribution unlimited.

17. DISTRIBUTION STATEMENT *(of the abstract entered in Block 20, if different from Report)*

18. SUPPLEMENTARY NOTES

This work sponsored by the Defense Nuclear Agency under RDT&E RMSS Code B325076464 V99QAXNA01102 H2590D.

19. KEY WORDS *(Continue on reverse side if necessary and identify by block number)*

Nuclear Fallout
Nuclear Weapons Effects
Fallout Modeling
Fallout Prediction
DELFIC

20. ABSTRACT *(Continue on reverse side if necessary and identify by block number)*

DELFIC predicts local fallout from nuclear weapon explosions in the yield range from 0.001 to 100,000 KT over a range of heights of burst from shallow subsurface to fallout-safe airbursts. The code is designed for research use and to serve as a comparison standard for production-oriented codes.

Physical and mathematical bases of the code and validation results are presented.

DD FORM JAN 73 1473 EDITION OF 1 NOV 65 IS OBSOLETE

UNCLASSIFIED

SECURITY CLASSIFICATION OF THIS PAGE *(When Data Entered)*

SUMMARY

DELFIC development began about fourteen years ago under Defense Atomic Support Agency sponsorship as a joint effort of the Army Nuclear Defense Laboratory, Naval Radiological Defense Laboratory and Technical Operations, Inc. Contributions from these organizations were patched together to form the initial version of the code. While it was functional, there was little consistency in structure and nomenclature between its various parts. Since then there have been many additions and deletions to the code, and the documentation, originally in seven volumes,[1-7] has been revised and incremented accordingly.[8-13] Thus, what began as a voluminously documented hodgepodge has become even more so in some respects.

To make DELFIC more useful to others, we have performed a thorough reorganization and clean-up of the code and documentation. Features of questionable value, or which simply have not been used, have been stripped away. A great amount of consolidation and reprogramming has been done. Consistency in code structure, data specification and nomenclature between modules has been improved. Perhaps most important, the documentation has been reduced to two volumes.

PREFACE

The author gratefully acknowledges the support and cooperation of Dr. David L. Auton of the Defense Nuclear Agency.

TABLE OF CONTENTS

TABLE OF CONTENTS (continued)

TABLE OF CONTENTS (continued)

LIST OF ILLUSTRATIONS

LIST OF TABLES

1. INTRODUCTION AND OVERVIEW

DELFIC (DEfense Land Fallout Interpretative Code) is intended for research in local nuclear fallout prediction and to serve as a standard against which predictions by less capable, production-oriented codes can be judged. By local fallout we mean the intensely radioactive material which falls to the ground within several to several hundred miles of ground zero, depending on the size of the explosion. The code is essentially open-ended with regard to input data, it is highly flexible in that it offers many options that would not be available in a production-oriented code, and it strives to include as much of the physics of fallout transport and activity calculation, without resorting to short cuts, as is practicable.

Calculation begins at about the time the fireball reaches pressure equilibrium with the atmosphere. Rise, growth and stabilization of the nuclear cloud is computed by a dynamic model that treats the cloud as an entraining bubble of hot air loaded with water and contaminated ground material. The fallout particle cloud, including the stem, is formed during the cloud rise. This calculation requires specification of a vertical profile of atmospheric data: pressure, temperature, humidity and wind; thus, the height, dimensions and vertically sheared horizontal displacement of a particular cloud are determined by the atmospheric stability and winds.

After cloud stabilization, representative parcels of fallout are transported through an atmosphere that is defined by input data. The user may specify a single vertical wind profile and assume a steady state. He may specify any number of wind profile updates. He may resolve the transport space in the horizontal and specify multiple wind profiles defined at different geographical locations, in which case winds in the cells of a three-dimensional space grid are determined by an interpolation procedure.

During transport, fallout parcels are expanded in the horizontal by ambient turbulence. Turbulence data may be input along with the winds, but since these data are rarely available, they can be calculated by the code.

To account for effects of vertical wind shear on the dispersion of individual parcels, tops and bases of the parcels are transported to ground impaction separately, and then recombined. The impacted parcels are distributed over the ground via a bivariate Gaussian function.

Any or all of sixteen unique quantities computed from the deposited fallout may be mapped. Radioactivity is calculated rigorously for any time by summing exposure or exposure rate contributions from all nuclides in the mixture of fission products. Any of twelve different types of fission may be specified. Induced activity in soil material in the fallout and in ^{238}U may be accounted for.

The remainder of this presentation is partitioned into four parts, in accord with the code structure. We begin with Initialization and Cloud Rise, proceed to Atmospheric Transport, then to Activity Calculation, and finally we discuss Map Preparation. The last chapter presents some validation results.

Volume II of this set is a user's manual.

2. INITIALIZATION AND CLOUD RISE

2.1 INITIALIZATION

2.1.1 Time, Temperature and Mass of Fallout

The cloud rise calculation is initialized at roughly the time when the fireball reaches pressure equilibrium with the atmosphere. Time and temperature as functions of yield and height of burst were determined from measurements made from cinefilms of nuclear cloud rise and from radiation measurements of fireballs. Details are given in ref. 2. Initial time, t_i (seconds) is

$$t_i = 56\, t_{2m} W^{-0.30} \quad , \tag{2.1.1}$$

where the time of the second temperature maximum, t_{2m} (seconds), is

$$t_{2m} = 0.037 \left(1.216^{\lambda/180}\right) W^{(0.49 - 0.07\lambda/180)}, \; 0 \leq \lambda \leq 180, \tag{2.1.2}$$

W is yield (KT) and λ scaled height of burst (ft $KT^{-1/3}$) (Subroutine TIMEE).

Initial gas temperature, T_i ($^{\circ}K$), is

$$T_i = K\left(\frac{t_i}{t_{2m}}\right)^n + 1500 \tag{2.1.3}$$

in which

$$K = 5980\ (1.145)^{\lambda/180}\ W^{(-0.0395+0.0264\lambda/180)}$$

and

$$n = -0.4473 W^{0.0436} \quad .$$

Temperature of condensed phase matter, $T_{s,i}$ (^{o}K), is conjectural but important since the energy required to heat it must be taken from that available. The following specification has been found to work satisfactorily

$$T_{s,i} = 200 \log_{10} (W) + 1000 \qquad (2.1.4)$$

where W is in kilotons. (Subroutine TEMP)

Mass of fallout, m_s (kg), (i.e., soil plus weapon debris) in the cloud at t_i is given for a subsurface burst with scaled depth of burst d(ft $KT^{-1/3.4}$) by

$$m_s = k_d W^{3/3.4} R(d)^2 D(d), \ 0 \le d \le 20 \qquad (2.1.5)$$

where

$$R(d) = 112.5 + 0.755d - 9.6 \times 10^{-6} d^3 - 9.11 \times 10^{-12} d^5$$

$$D(d) = 32.7 + 0.851d - 2.52 \times 10^{-5} d^3 + 1.78 \times 10^{-10} d^5,$$

and for surface and above surface bursts with scaled height of burst Λ(ft $KT^{-1/3.4}$) by

$$m_s = k_\Lambda W^{3/3.4} (180 - \Lambda)^2 \ (360 + \Lambda), \ 180 \ge \Lambda \ge 0. \qquad (2.1.6)$$

The constants k_d and k_Λ were determined from an analysis of Teapot Ess fallout to be 2.182 and 0.07741(kg ft^3) respectively. The scaling equation for subsurface bursts, eq. (2.1.5), is based on Nordyke's scaling function for high explosive cratering results,[14] and the above-surface scaling function, eq. (2.1.6), is based on the volume of intersection of a fireball with the ground.[2] (Subroutine MASS)

When $\Lambda > 180$ (ft $KT^{-1/3.4}$), we assume a "pure airburst" (i.e., the fireball does not touch the ground), and usually no local fallout is produced. In this case we take

$$t_{2m} = 0.045W^{0.42} \qquad (2.1.2')$$

and t_i is then calculated from eq. (2.1.1). Temperature is

$$T_i = K'(t_i/t_{2m})^n + 1500 \qquad (2.1.3')$$

where

$$K' = 6847W^{-0.0131}$$

and n is as for eq. (2.1.3). Mass of weapon debris is taken to be 90.7 kg.* (Subroutine AIRBRS)

2.1.2 Soil Solidification Temperature

Of great importance to the activity calculations (sec. 4.2.2) is the time after detonation when soil particles, which will constitute the bulk of the local fallout, cease to absorb radioactive fission products on their surfaces. In DELFIC this is taken to be the time the average cloud temperature reaches the so-called soil solidification temperature. The user may specify this

---

* Though during the cloud rise calculation all soil is taken to be in a condensed phase, an estimate of the partition of the soil burden between vapor and condensed phases is made and printed. Mass of vaporized soil at t_i, $m_{v,i}$ (kg), is computed via the conjectural equation

$$m_{v,i} = 0.00015m_s(T_i - T_m),$$

where T_m is 3000 °K for siliceous and 3100 °K for calcareous soils as these are defined in sec. 2.1.2. (Subroutine VAPOR)

temperature, or on default of input, the code will specify it. For this purpose we distinguish two types of soil: siliceous soil of continental (e.g., Nevada Test Site) origin (2200 ^{o}K), and calcarious soil of coral (e.g., Pacific Test Site) origin (2800 ^{o}K). On default of soil type specification, the code selects the continental type.

2.1.3 Mass and Geometry of the Cloud

On the basis of considerable experience with the cloud rise model we take the fraction of explosion energy used to heat air, soil and water to their initial temperatures to be 45% of the joule equivalent of the total yield, W. That is, the energy available to heat the cloud contents, H (joules), is

$$H = 0.45\ (4.18 \times 10^{12} W)$$

where W is in kilotons. To allow for situations where substantial amounts of water are taken into the fireball, the user may specify a number ϕ which is the fraction of H used to heat air and soil; the fraction $(1 - \phi)$ then is used to heat condensed water.

If the ambient temperature at the initial height of the cloud (eq. (2.1.13)) is $T_{e,i}$, then the masses of air and water in the cloud at t_i, $m_{a,i}$ and $m_{w,i}$(kg), are

$$m_{a,i} = \frac{\phi \left[H - m_s \int_{T_{e,i}}^{T_{s,i}} c_s(T)dT \right]}{\int_{T_{e,i}}^{T_i} c_{pa}(T)dT + x_e \int_{T_{e,i}}^{T_i} c_{pw}(T)dT} \qquad (2.1.7)$$

$$m_{w,i} = \frac{(1-\phi)\left[H - m_s \int_{T_{e,i}}^{T_{s,i}} c_s(T)dT\right]}{\int_{T_{e,i}}^{T_i} c_{pw}(T)dT + L} + x_e m_{a,i} \,. \qquad (2.1.8)$$

The total initial mass, m_i, and volume, V_i, of the cloud are

$$m_i = m_{a,i} + m_{w,i} + m_s \qquad (2.1.9)$$

$$v_i = (m_{a,i} + m_{w,i})\, R_a T_i^*/P \,. \qquad (2.1.10)$$

Here $c_s(T)$, $c_{pa}(T)$ and $c_{pw}(T)$ are specific heats of soil, air and water given by (joules kg^{-1} $^oK^{-1}$)

$$c_{pa}(T) = 946.6 + 0.19710T, \; T \leq 2300 \; ^oK$$

$$c_{pa}(T) = -3587.5 + 2.125T, \; T > 2300 \; ^oK$$

$$c_{pw}(T) = 1697.66 + 1.144174T$$

$$c_s(T) = 781.6 + 0.5612T - 1.881 \times 10^7/T^2, \; T \leq 848 \; ^oK$$

$$c_s(T) = 1003.8 + 0.1351T, \; T > 848 \; ^oK;$$

L is the latent heat of vaporization of water or ice, taken to be 2.5×10^6 and 2.83×10^6 joules kg^{-1} respectively; R_a is the ideal gas law constant for air (287 joules kg^{-1} $^oK^{-1}$);

$$x_e = H_R P_{ws}/(\varepsilon P) \qquad (2.1.11)$$

where H_R is relative humidity (fractional), $\xi = 29/18$ is the ratio of molecular weights of air and water, P is ambient pressure, P_{ws} is saturation water vapor pressure (Pa) given by

$$P_{ws} = 611(273/T_e)^{5.13} \exp\left[25(T_e - 273)/T_e\right] \qquad (2.1.12)$$

where T_e is ambient temperature (^oK); and T_i^* is virtual temperature (see the glossary in Appendix D) in the cloud at t_i.

The initial cloud is assigned the shape of an oblate spheroid with eccentricity 0.75. The eccentricity value 0.75 is an average, with standard deviation 0.08, found by Norment and Woolf for ten test shots that cover a yield range from 3.6 KT to 15 MT.[15] Norment and Woolf found little variation of eccentricity with height, particularly for small and medium yield shots, up to the altitude at which stabilization and final horizontal expansion begins. For a cloud with eccentricity 0.75, the ratio of vertical to horizontal cloud radii, H_e/R_e, is 0.66144. (Subroutine CRMINT)

2.1.4 Altitude and Speed

Good results are obtained with the initial cloud center altitude, z_i (m relative to sea level), given by

$$z_i = z_{GZ} + z_{HoB} + 90W^{1/3} . \qquad (2.1.13)$$

where z_{GZ} and z_{HoB} are altitudes of ground zero and height of burst above ground zero and W is yield (KT).

Initial rise speed, u_i (m s^{-1}), is

$$u_i = 1.2\sqrt{gR_{c,i}} \qquad (2.1.14)$$

where g = 9.8 is acceleration of gravity and $R_{c,i}$ is initial cloud radius. The

form of this equation results from a simple, approximate analysis of initial fireball rise, and the constant 1.2 is chosen to fit observed data. (Subroutine CRMINT)

2.1.5 Atmospheric Conditions

Height, radius and horizontal location relative to ground zero of the stabilized cloud* are sensitive to atmospheric stability and the ambient winds. The user provides single vertical profiles of atmospheric temperature, pressure, relative humidity and wind for use by the dynamic cloud rise. They also are used to compute particle settling and advection during the cloud rise such that by stabilization time, the particle cloud geometry is defined as functions of particle size and space above and downwind of ground zero. (Data input via subroutines ATMR and SHWIND)

Multiple wind profiles which may be used later for atmospheric transport (sec. 3.5) are not used here; a single wind profile is input especially for the cloud rise calculation.

In addition to pressure, temperature and humidity, the user also may input air density and viscosity, but in lieu of their input, the code computes them from the other quantities. Some flexibility of input is allowed: altitude, temperature and relative humidity must be specified, but either or both of pressure or density may be specified.

2.1.6 Particle Size Distribution

The user may specify one of three types of particle size distribution:

1. a lognormal distribution of number of particles with respect to diameter, specified in terms of median diameter and geometric standard deviation,

*Stabilization occurs when ambient transport and dispersion of the cloud becomes dominant over internally generated rise and expansion.

2. a power law distribution of particle mass fraction with respect to diameter, specified in terms of the power law exponent and a parameter k/m which is defined below, or

3. an arbitrary distribution of mass fraction with respect to particle diameter, specified by input of a table of values.

A lognormal distribution is selected by the code on default of user specification.

Lognormal Distribution[20]

The lognormal distribution is examined in some detail in Appendix A; here we present a brief summary. A particle distribution is said to be lognormal if the number of particles, $d\P(\delta)$, in the diameter range $d\delta$ centered on δ is given by

$$d\P(\delta) = \frac{1}{\sqrt{2\pi}\ \delta\ \ell n\ s}\ \exp\left[-\frac{1}{2}\left(\frac{\ell n\ \delta - \ell n\delta_{50}}{\ell n s}\right)^2\right] d\delta \qquad (2.1.15)$$

where δ_{50} and s are the median diameter and geometric standard deviation of the distribution.

For DELFIC calculations the user may specify δ_{50} and s*, or on default of specification, the code assigns the values

$$\delta_{50} = 0.407\ \mu m$$

$$s = 4.0\ ,$$

which are representative of Nevada Test Site fallout and are used for surface or near surface bursts ($\Lambda < 180$ ft $KT^{-1/3.4}$), while it assigns

*See Appendix A for a discussion of how to specify δ_{50} and s.

$$\delta_{50} = 0.15\ \mu m$$

$$s = 2.0$$

for pure air bursts ($\Lambda \geq 180$ ft $KT^{-1/3.4}$).[21]

A unique characteristic of the lognormal distribution is that the frequency functions for particle surface area and volume* are simply related to the frequency function for number. The surface area frequency with respect to diameter is obtained by replacing $\ell n\delta_{50}$ in eq. (2.1.15) with $\ell n\delta_{50} + 2(\ell ns)^2$, and the volume frequency by replacing $\ell n\delta_{50}$ in eq. (2.1.15) with $\ell n\delta_{50} + 3(\ell ns)^2$. Thus the median diameters for the surface and volume distributions corresponding to $\delta_{50} = 0.407\ \mu m$, $s = 4.0$ are 19 and 130 μm respectively, while those for $\delta_{50} = 0.15\ \mu m$, $s = 2.0$ are 0.39 and 0.63 μm. (Subroutines ICM and DSTBN)

Power Law Distribution

Power law distributions are mathematically meaningless since distribution functions cannot be defined for them. This is because the power law function is not properly bounded for zero argument. Freiling has shown that fallout particle distributions that have been represented by power law functions can equally well be fitted by lognormal distribution functions.[22] The implication of Freiling's work is that power law distributions would be more accurately described as truncated lognormal distributions. Nevertheless, power law distributions may be useful in fallout work.

Define the power law frequency as

$$d\pi(\delta|k,X) = k\delta^{-X}d\delta \quad , \tag{2.1.16}$$

where $d\pi(\delta|k,X)$ is the number of particles in the diameter range $d\delta$ centered on δ. If we assume spherical particles with constant density, ρ, we have

*Note that volume and mass distributions are equivalent for spherical particles whose densities are constant over the distribution.

$$dF\left(\delta \left| \frac{\pi\rho k}{6m_s}, X\right.\right) = \frac{\pi\rho k \delta^{3-X}}{6m_s}\, d\delta\,, \qquad (2.1.17)$$

where $dF\left(\delta \left| \frac{\pi\rho k}{6m_s}, X\right.\right)$ is the fraction of the total fallout mass, m_s, in the diameter range δ to $\delta + d\delta$.

The mass fraction of particles in the macro range from δ_i to δ_j is obtained by integration of eq. (2.1.17) between these limits to give

$$\Delta F = \frac{\pi\rho}{6(4-X)}\,(k/m_s)\left(\delta_j^{4-X} - \delta_i^{4-X}\right)\,, \quad 0 < X < 4. \qquad (2.1.18)$$

In DELFIC the power law distribution is specified by the exponential quantity X and the ratio k/m. Here we have dropped the subscript s from the mass since the ratio k/m would have been determined from one or more samples of fallout rather than from the entire mass of fallout. Details on data analysis and a description of the distribution in histogram form are given in Appendix B. (Subroutine DISTBN)

Tabular Distribution

Mass fraction and boundary particle diameters for each particle size class of a distribution histogram are specified by the user. The central particle diameter for the size class is taken to be the geometric mean of the boundary diameters. (Subroutine DSTBN)

Size-Activity Distribution

The user may specify any of the above to be a particle diameter-activity fraction distribution. For such a case the code selects an activity K factor (Roentgens m^2 hr^{-1} KT^{-1}) to match a user specified fission type, and a conventional, rather than rigorous, activity calculation ensues.

In effect this procedure also is used for pure air bursts, since DELFIC assumes that activity is uniformly distributed through the fallout particles, regardless of their size, for pure air bursts.

2.2 CLOUD RISE

2.2.1 Background

The DELFIC cloud rise model is based on the work of Huebsch[16,17] as modified by Norment.[8,13]. It provides a dynamic, one-dimensional, entraining bubble model of nuclear cloud rise, which is based on a set of coupled ordinary differential equations that represent conservation of momentum, mass, heat and turbulent kinetic energy. The nuclear cloud is defined in terms of: vertical coordinate of its center (the cloud is in some respects treated as a point),* cloud volume, average temperature, average turbulent energy density, and the masses of its constituents: air, soil and weapon debris, water vapor and condensed water. Cloud properties and contents are taken to be uniform throughout the cloud volume. The differential equations are solved by a fourth-order Runge-Kutta algorithm. (Subroutine RKGILL) Complete simulations use very little computer time.

Norment presents results of a validation study of the model.[13]

2.2.2 Differential Equations (Symbols are defined in the Glossary found in Appendix D.)

Momentum

$$\frac{du}{dt} = \overset{(a)}{\left(\frac{T^*}{T_e^*}\,\beta' - 1\right)}g - \overset{(b)}{\left(\frac{2k_2 v}{H_c}\,\frac{T^*}{T_e^*}\,\beta'\right)} + \overset{(c)}{\left(\frac{1}{m}\,\frac{dm}{dt}\right)}u \qquad (2.2.1)$$

*Effects of this model limitation on rise simulation of very large clouds are discussed in sec. 4 of ref. 13.

Terms (a), (b) and (c) represent forces due to buoyancy, eddy-viscous drag and entrainment drag respectively.

k_2 is a dimensionless parameter that has been calibrated to give satisfactory simulation results as:

$$k_2 = \max\left[0.004, \min(0.1, 0.1W^{-1/3})\right] . \qquad (2.2.1a)$$

In long form, this equation means:

$$k_2 = 0.1 \quad , \quad W < 1 \text{ KT}$$

$$k_2 = 0.1W^{-1/3}, \quad 1 \leq W \leq 15{,}625 \text{ KT}$$

$$k_2 = 0.004 \quad , \quad 15{,}625 < W \text{ KT} \quad .$$

The characteristic velocity, v, is

$$v = \max(u, \sqrt{2E}) . \qquad (2.2.1b)$$

Center Height

$$\frac{dz}{dt} = u \qquad (2.2.2)$$

Temperature

Dry (water is not condensed)

$$\frac{dT}{dt} = -\frac{\beta'}{\bar{c}_p(T)}\left[\overset{(a)}{\frac{T^*}{T_e^*}gu} + \overset{(b)}{\left(\int_{T_e}^{T} c_{pa}(T)dT\right)\frac{1}{\beta' m}\frac{dm}{dt}\bigg|_{ent}} - \overset{(c)}{\varepsilon}\right] \qquad (2.2.3D)$$

where $\bar{c}_p(T) = \beta' c_p(T) + (1 - \beta')c_s(T)$ and where $c_p(T) = [c_{pa}(T) + xc_{pw}(T)]/(1 + x)$. Terms (a), (b) and (c) account for the effects of adaibatic expansion, entrainment and dissipation of turbulent energy to heat respectively.

Wet (water is condensed)

$$\frac{dT}{dt} = -\frac{\beta'}{1 + \frac{L^2 x \xi}{c_p R_a T^2}} \left[\left((T - T_e) + \frac{L(x - x_e)}{c_p} \right) \frac{1}{m\beta'} \left. \frac{dm}{dt} \right|_{ent} + \frac{T^*}{T_e^*} \frac{g}{c_p} u \left(1 + \frac{Lx}{R_a T} \right) - \frac{\varepsilon}{c_p} \right] \qquad (2.2.3W)$$

Turbulent Kinetic Energy Density

$$\frac{dE}{dt} = \underset{(a)}{2k_2 \frac{T^*}{T_e^*} \beta' \frac{u^2 v}{H_c}} + \underset{(b)}{\frac{u^2}{2} \frac{1}{m} \left. \frac{dm}{dt} \right|_{ent}} - \underset{(c)}{E \frac{1}{m} \left. \frac{dm}{dt} \right|_{ent}} - \underset{(d)}{\varepsilon} \qquad (2.2.4)$$

Terms (a) and (b) account for turbulent energy generated by the mean flow via eddy-viscous drag and momentum-conserving inelastic-collision entrainment respectively. Term (c) represents entrainment dilution, and (d) represents dissipation to heat, where the turbulence dissipation rate, ε, is

$$\varepsilon = \frac{k_3 (2E)^{3/2}}{H_c} \qquad (2.2.4a)$$

k_2 and v are given by eqs. (2.2.1a, b) and k_3 is a dimensionless constant of value 0.175.

Mass

Dry (water is not condensed)

$$\left.\frac{dm}{dt}\right|_{ent} = \frac{\beta' m}{1 - \frac{\beta'}{T^* \bar{c}_p} \int_{T_e}^{T} c_{pa}(T)dT}$$

$$\cdot \left\{ \underset{(a)}{\frac{S}{V}\mu v} + \frac{\beta'}{T^* \bar{c}_p} \underset{(b)}{\left[\frac{T^*}{T_e^*} gu\right]} - \underset{(c)}{\varepsilon} \right] - \underset{(d)}{\frac{gu}{R_a T_e^*}} \right\} \quad . \qquad (2.2.5D)$$

This equation is based on observed volumetric growth of nuclear clouds, and term (a) contains this information. The other terms are required to convert volumetric to mass growth rate. Terms (b) and (c) account for temperature effects caused by entrainment and conversion of turbulence energy to heat; term (d) accounts for hydrostatic expansion of the rising cloud.

Wet (water is condensed)

$$\left.\frac{dm}{dt}\right|_{ent} = \frac{\beta' m}{1 - \frac{1}{T^*}\left[\frac{\beta'}{1 + \frac{L^2 x \xi}{c_p R_a T^2}}\right]\left[T - T_e + \frac{L(x - x_e)}{c_p}\right]}$$

$$\cdot \left\{ \frac{S}{V}\mu v + \frac{\beta'/T^*}{1 + \frac{L^2 x \xi}{c_p R_a T^2}} \left[\frac{guT^*}{T_e^* c_p}\left(1 + \frac{Lx}{R_a T}\right) - \frac{\varepsilon}{c_p}\right] - \frac{gu}{R_a T_e^*} \right\}. \qquad (2.2.5W)$$

Equations (2.2.5D and W) account for mass change by entrainment of ambient air only. The net change must also account for fallout at rate F to give

$$\frac{dm}{dt} = \left.\frac{dm}{dt}\right|_{ent} - F \quad . \tag{2.2.5}$$

Good results are obtained when the dimensionless entrainment parameter μ is given by

$$\mu = \max\left[\max(0.12,\ 0.1W^{0.1}),\ 0.01W^{1/3}\right] \quad . \tag{2.2.5a}$$

In long form this equation means:

$$\mu = 0.12 \quad , \quad W \leq 6.192 \text{ KT}$$

$$\mu = 0.1W^{0.1} \quad , \quad 6.192 \leq W \leq 19{,}307 \text{ KT}$$

$$\mu = 0.01W^{1/3} \quad , \quad 19{,}307 \leq W \text{ KT} \quad .$$

Soil Mass Mixing Ratio

$$\frac{ds}{dt} = \underbrace{-\frac{1}{\beta'}\frac{1+x}{1+x_e}\, s\, \frac{1}{m}\left.\frac{dm}{dt}\right|_{ent}}_{(a)} \underbrace{-\frac{1+x+s+w}{m}\left(\frac{s}{s+w}\right)F}_{(b)} \tag{2.2.6}$$

Term (a) accounts for entrainment dilusion, and term (b) accounts for fallout from the cloud.

Water Vapor Mixing Ratio

Dry (water is not condensed)

$$\frac{dx}{dt} = -\frac{1+x+s}{1+x_e}\,(x - x_e)\,\frac{1}{m}\left.\frac{dm}{dt}\right|_{ent} \quad . \tag{2.2.7D}$$

Wet (water is condensed, x is the saturation mixing ratio)

$$\frac{1}{x}\frac{dx}{dt} = (1 + x/\varepsilon)\frac{L\varepsilon}{R_a T^2}\frac{dT}{dt} + (1 + x/\varepsilon)\frac{g}{R_a T_e^*}u \quad . \qquad (2.2.7W)$$

Condensed Water Mixing Ratio

$$\frac{dw}{dt} = -\frac{1}{\beta'}\left(\frac{1 + x}{1 + x_e}\right)\underbrace{\left(w + x - x_e\right)\frac{1}{m}\frac{dm}{dt}\bigg|_{ent}}_{(a)} - \underbrace{\frac{dx}{dt}}_{(b)} \quad . \qquad (2.2.8)$$

Term (a) accounts for entrainment dilusion and term (b) accounts for condensation of water vapor in the cloud. Fallout of condensed water is neglected. (Subroutine DERIV)

2.2.3 Particle Settling

Particle settling speeds are needed to compute fallout from the cloud during rise and later to define in detail the stabilized particle cloud and to compute trajectories of individual particles from the cloud to ground impaction. For these purposes DELFIC computes still-air, terminal, gravity settling speeds of spherical particles. Atmospheric properties at the particle altitude are obtained by interpolating in the tables of data supplied by the user (sec. 2.1.5). Particle density is either specified by the user or set by the code to 2600 kg m^{-3}.

The calculations are generalized in terms of the dimensionless Davies number, N_D,

$$N_D = 4\rho\,(\rho_p - \rho)g\,\delta^3/(3\eta^2) \qquad (2.2.9)$$

where ρ and ρ_p are air and particle densities, δ is particle diameter, η is air viscosity and g is acceleration of gravity. Still-air, terminal settling speed, f, is, according to Stokes' law for small N_D,

$$f = \eta N_D s/(24\rho\delta) \ , \ N_D \leq 0.3261 \ . \qquad (2.2.10a)$$

For intermediate N_D use Beard's[18] equation

$$f = \frac{\eta s}{\rho\delta} \exp\left[- 3.18657 + 0.992696Y - 0.153193 \times 10^{-2}Y^2 - 0.987059 \times 10^{-3}Y^3 \right.$$

$$\left. - 0.578878 \times 10^{-3}Y^4 + 0.855176 \times 10^{-4}Y^5 - 0.327815 \times 10^{-5}Y^6 \right] ,$$

$$0.3261 < N_D \leq 84.175 \qquad (2.2.10b)$$

where $Y = \ell n(N_D)$. For large N_D use Davies'[19] equations:

$$f = \eta N_D s \left(4.166667 \times 10^{-2} - 2.3363 \times 10^{-4}N_D \right.$$

$$\left. + 2.0154 \times 10^{-6}N_D^2 - 6.9105 \times 10^{-9}N_D^3\right)/(\rho\delta), \ 84.175 < N_D < 140, \qquad (2.2.10c)$$

$$\log_{10}(f\rho\delta/\eta) = - 1.29536 + 0.986X$$

$$- 0.046677X^2 + 1.1235 \times 10^{-3}X^3, \ 140 \leq N_D < 4.5 \times 10^7 \ , \qquad (2.2.10d)$$

where $X = \log_{10}(N_D)$, and the slip factor in eqs. (2.2.10a), (2.2.10b) and (2.2.10c) is

$$s = 1.0 + 54.088\eta T^{1/2}/(\delta P) \ , \qquad (2.2.11)$$

where P and T are air pressure and temperature. (Subroutine SETTLE)

2.2.4 Cloud Shape and Volume

Initially the cloud is given the shape of an oblate spheroid of eccentricity 0.75 (sec. 2.1.3). This shape is maintained until the cloud stops rising, after which the vertical thickness of the cloud remains constant, and further volume growth, if any, is accommodated by lateral expansion. The cloud volume at any time is computed via

$$V = R_a T^* \beta' m / P. \tag{2.2.12}$$

(Subroutine RKGILL)

2.2.5 Effect of Wind Shear

To account for effects of wind shear, simple adjustments are made to the volume terms in eqs. (2.2.5D) and (2.2.5W). Namely,

$$\frac{S}{V}\,\mu v \rightarrow \mu\left(\frac{S}{V}\,v + k_6\,\frac{1.5}{R_c}\,v_s\right) \tag{2.2.13}$$

where v_s is the magnitude of the wind velocity difference between the top and base of the cloud cap, and k_6 is a dimensionless constant taken to be unity. (Subroutine DERIV)

2.2.6 Termination of Cloud Rise and Expansion

There are two normal termination switches, and stabilization is taken to occur as soon as one of these is tripped:

a. The R-RATE switch is tripped when

$$\frac{|\Delta R_c|}{\Delta t} \leq \frac{R_c W^{0.014778}}{1153} \quad \text{and } u = 0. \tag{2.2.14a}$$

b. The U, EK switch is tripped when

$$E < \max \left[10, \min (23 + 9 \log_{10} W, 60)\right] \text{ and } u = 0. \qquad (2.2.14b)$$

In long form, relation (2.2.14b) means that termination occurs when

$$E < 10 \quad , \quad W \leq 0.0359 \text{ KT}$$

$$E < 23 + 9\log_{10} W \quad , \quad 0.0359 \leq W \leq 12{,}915 \text{ KT}$$

$$E < 60 \quad , \quad 12{,}915 \leq W \text{ KT}$$

and

$$u = 0.$$

Here E is in units of joules kg^{-1} (i.e., $m^2 s^{-2}$). It turns out that most low and medium yield cases are terminated by this switch, but megaton yield cases are terminated by the R-RATE switch. (Subroutine CXPN)

2.3 DEFINITION OF THE PARTICLE CLOUD

The set of coupled differential equations described in sec. 2.2 are integrated from time t_i to cloud stabilization such as to provide a complete history of the cloud rise and growth. During this calculation, cloud properties are tabulated at intervals in an array CX, the cloud history table, which appears in the printed output (II, p. 42). (Subroutine CXPN)

To define the particle cloud, the cloud rise and growth is resimulated for each particle size by passing through the CX array. Thus, a separate particle cloud is defined for each size. At time t_i, each cloud is taken to have uniform composition and a cylindrical shape which is subdivided in the

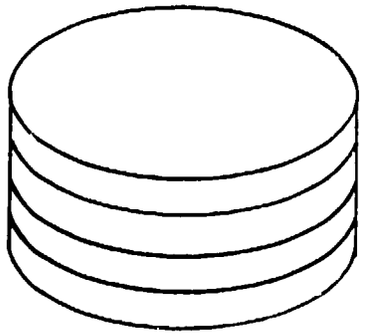

Figure 1. Subdivision of an initial cloud cylinder into four parcels, KDI = 4.

vertical into KDI cylindrical parcels as illustrated in Fig. 1. The diameter and height of the cylindrical cloud are taken equal to the major and minor axes of the spheroidal cloud. KDI is either specified by the user or assigned the value

$$KDI = 15 + \ell n(W) \qquad (2.3.1)$$

where W is yield in kilotons.

During the resimulated cloud rise it is necessary to distinguish between the cloud cap, which has properties as recorded in the CX table, and the particle cloud which is being calculated. Gravity settling of the particles separates them from the cap such that the cap and particle clouds are distinct at all times subsequent to t_i, and the geometry of the particle cloud as displayed in Fig. 1 applies only at t_i.

As the CX table is passed, the code computes the height and diameter of the base and top of each parcel as follows. Particle settling speed, f, for actual conditions (in or below the cloud cap) is calculated (sec. 2.2.3), and to this is subtracted an upward component, u_u, which represents the influence of the cloud cap rise on the particle.

a. In-cloud

$$u_u = u_B + (z - z_B)\left(\frac{u_T - u_B}{z_T - z_B}\right) \qquad (2.3.2a)$$

b. Below-cloud

$$u_u = u_B\left(1 - \frac{z_B - z}{z_B - z_{GZ}}\right) \qquad (2.3.2b)$$

where u_T and u_B are the rates of rise of the cloud cap top and base, z is the parcel base or top altitude, z_T and z_B are the altitudes of cloud cap top and base and z_{GZ} is the altitude of the ground. The altitude of the parcel base or top is computed by point-slope integration of the equation

$$\frac{dz}{dt} = u_u - f$$

over each time increment of the CX table.

A parcel top or base which is inside the cloud cap is assigned the cap radius as recorded in the CX table. When the parcel base or top falls through the base of the cloud cap, it is assigned the cloud cap radius at the time of its fallout, and it keeps this radius thereafter. At stabilization time, the base and top of each parcel is examined to determine if either or both are below the cloud base. If not, the parcel is assigned the cloud cap stabilization radius. If one or both are below the cloud base, the parcel is subdivided into n parcels where

$$n = \mathrm{INT}(R_T/R_B);\ 2 \le n \le 10 \qquad (2.3.3)$$

and R_T and R_B are the radii of the parcel top and base. Each parcel subdivision is taken to have equal vertical thickness and equal mass. The radius R of a parcel subdivision at altitude z is computed by the geometric interpolation formula

$$R = R_B \left[\left(\frac{R_T}{R_B} \right)^{\frac{z - z_B}{z_T - z_B}} \right];\ z_B \le z \le z_T \qquad (2.3.4)$$

where all quantities are as defined above. The radius of the ith parcel subdivision, whose top and base are at altitudes z_i and z_{i-1}, is computed from eq. (2.3.4) for the altitude of its center of mass, z_{cm_i}, which is

$$z_{cm_i} = z_B + \frac{z_T - z_B}{2\ell n\left(\frac{R_T}{R_B}\right)} \ell n \left[0.5 \left\{ \left(\frac{R_T}{R_B}\right)^{\frac{2(z_i - z_B)}{(z_T - z_B)}} + \left(\frac{R_T}{R_B}\right)^{\frac{2(z_{i-1} - z_B)}{(z_T - z_B)}} \right\} \right] . \qquad (2.3.5)$$

(Subroutine RSXP)

Each parcel of fallout also may be subdivided in the horizontal as controlled by input parameter IRAD. While the code retains this capability, it has not proven to be useful and will not be discussed further here. On default of input of IRAD, no horizontal subdivision occurs. Details are given on pp. 56-58 of ref. 8.

To account for effects of advection and vertical wind shear on the horizontal disposition of the particle cloud, the CX table is again passed, this time backwards for each fallout parcel. The vertical trajectory of the parcel is thus recreated and its horizontal position is adjusted according to the time it spends in each wind stratum (sec. 2.1.5). (Subroutine WNDSFT)

Each fallout parcel and subparcel is defined by the following data which are passed on to the Diffusive Transport Module:

1. horizontal space coordinates of the parcel center
2. base altitude
3. time (stabilization time)
4. vertical thickness
5. radius
6. mass (or activity)
7. particle diameter
8. volume

The aggregate of these parcel descriptions represent the particle cloud, which includes the stem.

3. ATMOSPHERIC TRANSPORT

3.1 GENERAL DISCUSSION

The Initialization and Cloud Rise Module passes on to the Diffusive Transport Module (DTM) fallout parcel descriptions as discussed at the end of the preceeding section, plus vertical profiles of atmospheric pressure, temperature, humidity, density and viscosity. Wind data are supplied to the DTM as either: a single vertical profile, a sequence of single vertical profiles used to update the windfield and/or multiple profiles to account for variation of wind with geographic location. If the latter option is chosen, the user must also specify a three-dimensional grid which spans the atmospheric transport space along with parameters used for wind field interpolation, and vertical as well as horizontal wind components are considered.

During transport the fallout parcels are dispersed by ambient atmospheric turbulence. A scale-dependent method, corrected for effects of gravity settling, is used. Turbulence data may be specified by the user in a manner similar to that used for wind, or it can be computed by the code either as a simple function of altitude, or as a function of altitude on the basis of surface data specified by the user.

To account for differences in wind, turbulence and settling speed over the vertical span of individual fallout parcels, the tops and bases of the parcels are transported separately from the stabilized cloud to the ground. After ground impaction, the bases and tops are recombined to form a single deposit increment of fallout such as to reflect the dispersion between them during transport. This ensures reasonably accurate fallout prediction even when few parcels are transported. Furthermore, n + 1 transport calculations are required for n parcels, which is only one more than required for transport of parcel center points alone.

3.2 ADVECTION

There are two optional modes of transport: a more accurate but more time-consuming "layer-by-layer" method which computes transport through each vertical wind field stratum in a stepwise manner, and a "quick" method which computes transport in single steps from initial points to impact (or to time or space grid boundaries). In any case, particle settling speed is computed by subroutine SETTLE for each vertical stratum using atmospheric properties for that stratum for each particle size. As noted above, fallout parcel bases and tops are transported independently.

3.2.1 Layer-By-Layer Transport

For a general case, with temporally and spatially resolved winds, we have

$$\vec{r}(t_d) = \vec{r}(t_s) + \sum_{z_i}^{z_g} \frac{\vec{U}(x,y,z,t)\,\Delta z}{|w(x,y,z,t) - f(z)|} \qquad (3.2.1)$$

where $\vec{r}(t_s)$ is the initial horizontal location vector of the parcel top or base center, z_i is its initial altitude, $\vec{r}(t_d)$ is the horizontal location vector of the parcel base or top after impaction on the ground at altitude z_g, $\vec{U}(x,y,z,t)$ is the horizontal wind, $w(x,y,z,t)$ is the vertical wind component, $f(z)$ is particle settling speed, and the summation is taken over vertical wind strata of (variable) depth Δz through which the particle passes. Horizontal spatial resolution of the wind field is achieved by defining wind vectors at the centers of a three-dimensional space grid. The code is provided with an interpolation procedure which computes the grid cell wind vectors from an arbitrary set of spatially resolved input data. Temporal resolution is provided by updating the complete wind field at user specified intervals. (Subroutine TRANP)

3.2.2 Quick Transport

Quick transport is allowed only if all vertical wind components are taken to be zero. Wind data are presummed over the vertical wind strata according to

$$\vec{S}_j = \sum_{k=1}^{j} \vec{U}_k \, \Delta z_k \qquad (3.2.2)$$

where $\vec{S}_j$ is the vector sum stored for the jth wind stratum, $\vec{U}_k$ is the wind for the kth stratum of depth Δz_k, and the summation is taken from the surface stratum, k = 1, to the jth stratum. Similar summations are stored for the turbulence data and for the wind vector angle relative to the easterly direction. (Subroutine SUMDAT)*

During quick transport, we require the average wind $< \vec{U} >_{j,k}$ between the bases of strata j and k. This is obtained (Subroutine GETDA) via equation

$$< \vec{U} >_{j,k} = (\vec{S}_{k-1} - \vec{S}_j)/(z_{B,k} - z_{B,j}) \ , \ j < k, \qquad (3.2.3)$$

where $z_{B,j}$ is the altitude of the base of the jth stratum, etc. Similar equations apply for turbulence and angle. By making use of a precalculated table of deposition times from each stratum base, T, we have for a simple case that does not involve space or time boundaries

$$\vec{r}(t_d) = \vec{r}(t_i) + \vec{U}_k(z_i - z_{B,k})/f(k) + T_k < \vec{U} >_{1,k} \ , \qquad (3.2.4)$$

where f(k) is particle settling speed and $\vec{U}_k$ is wind in the kth stratum and other quantities are as previously defined. For cases where there is resolution in space or time, partial stratum transport terms, such as the middle

*The wind, turbulence and angle arrays are replaced by these sums. When individual quantities are desired, for example for layer-by-layer transport, they are retrieved by calculation from the summed quantities. (Subroutine GETDA)

term on the right side of eq. (3.2.4), are computed on both sides of a boundary whenever it is crossed. Thus, for finely resolved cases, this mode may lose much of its computational advantage, and the more accurate layer-by-layer method should be used.

3.3 TURBULENT DISPERSION

During and subsequent to atmospheric transport, fallout parcels are taken to have Gaussian distributions in the horizontal. As the parcel is subjected to the dispersive action of the turbulent atmosphere, the variance, σ^2, of the distribution grows accordingly. The pertinent measure of turbulence is turbulence energy density dissipation rate, $\varepsilon(m^2s^{-3})$, which is the quantity stored in the turbulence data arrays.* In accord with the Kolmogoroff-Batchelor theory of scale dependent Lagrangian diffusion of a puff of inert material by homogenious turbulence as formulated by Walton,[23] the parcel variance at time t is

$$\sigma(t)^2 = \left[\sigma(t_s)^{2/3} + \frac{2}{3}c\varepsilon^{1/3}(t - t_s)\right]^3 ; \ \sigma(t_s) \le \sigma(t) \le \sigma_\ell \qquad (3.3.1a)$$

$$\sigma(t)^2 = \sigma_\ell^2 \left\{2c(t - t_s)(\varepsilon/\sigma_\ell^2)^{1/3} + 3\left[\sigma(t_s)^2/\sigma_\ell^2\right]^{1/3} - 2\right\}; \ \sigma(t) > \sigma_\ell \qquad (3.3.1b)$$

where

$$c = \left[1 + \left(\frac{nT_L < f >}{D_E}\right)^2\right]^{-1/2} , \qquad (3.3.2)$$

σ_ℓ^2 is the parcel variance when its dispersion rate becomes constant, taken to be $10^9 m^2$ (this value is quite uncertain), and $\sigma(t_s)$ is the parcel standard deviation at cloud stabilization time, taken to be one-half the parcel radius

*Turbulence data arrays are congruent with the wind data arrays.

supplied by the Initialization and Cloud Rise Module. c is a correction for particle settling derived by Csanady,[24] where $< f >$ is altitude-averaged particle settling speed, T_L is the Lagrangian time scale of turbulence, D_E is Eulerian length scale of turbulence and n has values 1 and 2 for downwind and crosswind turbulence respectively. Good results are obtained with $T_L = D_E$.*

Turbulence data, in the form of ε values, may be specified by the user in the same manner as the winds are specified. However, since these data rarely will be available, the code can provide representative vertical profiles of horizontally isotropic ε via the method of Wilkins.[26]

Wilkins finds that ε can be approximated by a simple hyperbolic function of height above ground, z, by

$$\varepsilon = \frac{(\tau_o/\rho)^{3/2}}{k(z + z_o)} \quad , \tag{3.3.3}$$

where τ_o is atmospheric surface layer shearing stress, ρ is air density, $k = 0.35$, and z_o is surface roughness length.

---

*Actually, we should have $T_L/D_E = \beta/\sigma_w$ where $\beta \simeq 4$ is the ratio of Lagrangian to Eulerian turbulence time scales and σ_w is the standard deviation of vertical turbulence. According to Chen,[25] for example, $\sigma_w = 5.39\varepsilon^{1/3}$, so we have

$$c = \left[1 + (0.74n < f > \varepsilon^{-1/3})^2\right]^{-1/2} \tag{3.3.2'}$$

Since $\varepsilon^{-1/3}$ is typically in the range 10 to 100, this correction tends to decrease the dispersion rate to unrealistically low levels. While the code provides an option to use this equation (with a spatially and temporally averaged ε), normally we take $T_L/D_E = 1$ as noted above.

Equation (3.3.3) also can be written

$$\varepsilon = \frac{u_*^3}{k(z + z_o)} \quad , \tag{3.3.4}$$

where u_* is surface layer friction velocity given by

$$u_* = k\, u_s / \left[\ell n(s/z_o) + \psi_m \right] .$$

Here u_s is surface wind speed measured at height s (usually s = 10 meters), and ψ_m has the following empirical functional forms[27] of height and Monin-Obukhov Length, L:

a. stable conditions

$$\psi_m = 4.7\ s/L \ ;\ L > 0$$

b. neutral conditions

$$\psi_m = 0 \ ;\ L = \infty$$

c. unstable conditions

$$\psi_m = - \ell n\left[(\xi^2 + 1)(\xi + 1)^2/8\right] + 2 \tan^{-1}(\xi) - \frac{\pi}{2} \ ;$$

$$\xi = (1 - 15\ s/L)^{1/4} ;\ L < 0.$$

The user can input to DELFIC values for u_s, s, z_o and 1/L, and the code computes ε via eq. (3.3.4) at the altitude of each vertical wind stratum. Typical values of z_o are given by Pasquill,[28] and 1/L values are given by Golder.[29]

For many predictions it is sufficient to let the code set the parameters in eq. (3.3.4). In this case, typical (or "average") values of ε are computed via

$$\varepsilon = 0.03/z \ (m^2 s^{-3}) \tag{3.3.5}$$

3.4 DEPOSIT INCREMENT DESCRIPTION

As already noted, the base and top of each fallout parcel are independently transported from their position in the stabilized cloud to ground impact. Once impacted, the [illegible] recombined to define a deposit increment of fallout distributed over the impact plane by a bivariate Gaussian function.

Figure 2 illustrates how the distribution parameters of the base (subscript b) and top (subscript t) wafers are synthesized to yield the deposit increment distribution parameters. The subscript quantities $_{\parallel}$ and $_{\perp}$ are used to distinguish alongwind from crosswind standard deviations. The ellipse orientation angles, α_b and α_t, are the wind vector angles (relative to east) averaged over the particle trajectory by a procedure analogous to that used for the wind (eq. (3.2.3)). The deposit increment ellipse is the large, heavy lined ellipse. The deposit increment distribution parameters are computed from

$$\alpha = \arctan\left(\frac{y_t - y_b}{x_t - x_b}\right) \tag{3.4.1}^*$$

*Since the FORTRAN arctan subroutine yields α in the range $\pm \pi/2$, it is necessary to add the statement

```
IF(XT - XB • LT • 0.0) ALPHA = ALPHA - SIGN(3.141592654,ALPHA)
```

to extend the range to $\pm \pi$.

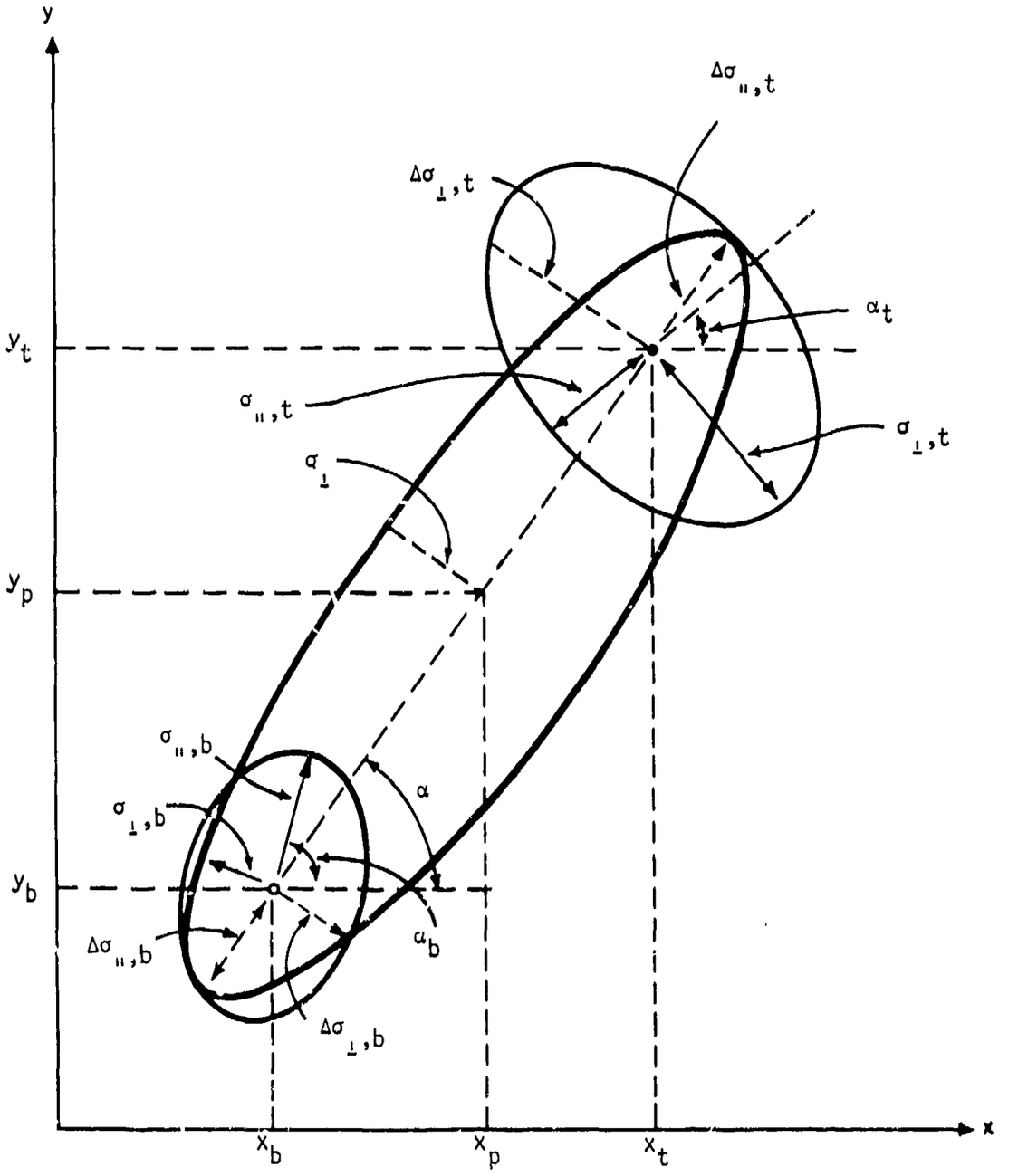

Figure 2. Illustration of the synthesis of a deposit increment from the standard deviation ellipses of the top and base of a parcel of fallout.

$$\Delta\sigma_{\parallel,b} = \left(\frac{\cos^2(\alpha_b - \alpha)}{\sigma^2_{\parallel,b}} + \frac{\sin^2(\alpha_b - \alpha)}{\sigma^2_{\perp,b}} \right)^{-1/2}$$

$$\Delta\sigma_{\perp,b} = \left(\frac{\sin^2(\alpha_b - \alpha)}{\sigma^2_{\parallel,b}} + \frac{\cos^2(\alpha_b - \alpha)}{\sigma^2_{\perp,b}} \right)^{-1/2} .$$

$\Delta\sigma_{\parallel,t}$ and $\Delta\sigma_{\perp,t}$ are computed similarly, and

$$\sigma_{\parallel} = \frac{1}{2}\left[\Delta\sigma_{\parallel,b} + \Delta\sigma_{\parallel,t} + \sqrt{(x_t - x_b)^2 + (y_t - y_b)^2}\right]$$

$$\sigma_{\perp} = \sqrt{\Delta\sigma_{\perp,b}\,\Delta\sigma_{\perp,t}} \qquad (3.4.2)$$

$$x_p = x_b + (\sigma_{\parallel} - \Delta\sigma_{\parallel,b})\cos\alpha$$

$$y_p = y_b + (\alpha_{\parallel} - \Delta\sigma_{\parallel,b})\sin\alpha \qquad (3.4.3)$$

The time recorded with the deposit increment is taken to be the arithmetic average of the impact times of the base and top. (Subroutine ADVEC) The center coordinates, x_p, y_p, standard deviations, $\sigma_{\perp}$, $\sigma_{\parallel}$, orientation angle, α, and other properties received from the Initialization and Cloud Rise Module, are passed along to the Output Processor Module where contributions in the deposition plane are computed by eq. (5.2.1).

3.5 WINDFIELD DESCRIPTION

3.5.1 Single Profile Windfields

Windfields that are horizontally homogenious are defined by single vertical profiles of two-dimensional wind vectors. (Vertical components are taken to be zero.) The atmosphere is stratified into layers based on the altitude increments at which the data are specified by the user. Limiting horizontal boundaries of the transport space also are specified.

Temporally resolved winds may be of this type; the winds are replaced by updates at specified time intervals. The only restriction is that the data must be specified at the same altitudes in all updates. (Subroutines DATIN and ONEDIN)

3.5.2 Multiple Profile Windfields

Horizontally nonhomogenious windfields, that is winds that vary with geographical location, are specified by multiple vertical profiles of winds which may be three-dimensional. (If vertical components are to be considered in single profile windfields, the methods of this section must be used.) Multiple profile windfields also may be time resolved.

The user must specify a three-dimensional space grid, for each cell of which a three-dimensional wind vector is to be defined by the code on the basis of the input data. A table of vertical strata center or base altitudes is specified, and these strata levels are held constant throughout the transport space. (Subroutine LAYERS) For the horizontal, a rectangular "control" net is specified in terms of: the coordinates of its south-west corner, a (square) mesh spacing, and indices which represent the numbers of mesh units to the east and north. Each control net mesh may be quartered, each quarter may be quartered, and so on (Vol. II, Fig. A.1). An identical net applies at each vertical stratum. (Subroutine GETUP)

Consider a general wind or turbulence component whose value, $D^{(n)}$, at the center of the nth atmosphere space cell is to be determined from the set of M specified components, D_i, i = 1,2,3,...,M. Here each D_i is defined at an arbitrary point in the atmosphere space. To determine $D^{(n)}$ we specify an integer N and two distances, α and β, and then the code computes

$$D^{(n)} = \sum_{i=1}^{N} g_i D_i \tag{3.5.1}$$

where the summation is over the N data with the largest g_i, where

$$g_i = \frac{\left(\frac{\alpha^2 - z_i^2}{\alpha^2 + z_i^2}\right)\left(\frac{\beta^2 - x_i^2 - y_i^2}{\beta^2 + x_i^2 + y_i^2}\right)}{\sum_{k=1}^{N}\left(\frac{\alpha^2 - z_k^2}{\alpha^2 + z_k^2}\right)\left(\frac{\beta^2 - x_k^2 - y_k^2}{\beta^2 + x_k^2 + y_k^2}\right)} \quad . \tag{3.5.2}$$

Here α and β are limiting distances in the vertical and horizontal respectively. Any terms in the g_i that are computed to be negative are set to zero. This weighting method is similar to one developed for similar use by Cressman.[30] (Subroutines DATIN and TRIDIN)

4. ACTIVITY CALCULATION

4.1 GENERAL DISCUSSION

Radioactivity calculations at three levels of sophistication are available in DELFIC:

1. Rigorous calculations that sum contributions from all nuclides in a decay chain. Decay from detonation to the requested time is computed for each nuclide by the Bateman equation (eq. (4.2.1)), and each activity is multiplied by a unique factor to convert to exposure rate; this eliminates the need to use a power law decay factor which is applicable to the mixed fission products. Radiochemical fractionation is accounted for in distributing activity with respect to particle size, and activity from individual mass chains can be predicted and mapped. A conventional K factor (i.e., exposure rate at H + 1 hour over fallout from one kiloton of fission yield spread uniformly over unit area) is not used by this method, but one can be, and is, calculated. (Subroutines PAM1, PAM2, BATMAN, GXPSR, INDCD2, MCHDEP and URAN)

2. The rigorous calculation is done for H + 1 hour, and then a $t^{-1.26}$ decay factor is used for subsequent times. This option is offered to save computer time in computing integrated exposure (dose) when time of arrival of individual fallout parcels is accounted for. A completely rigorous calculation requires repetition of the entire procedure for each fallout parcel, and can be expected to use a lot of computer time.

3. For pure air bursts, and particle distributions specified in terms of size-activity fraction, K factors and the $t^{-1.26}$ decay factor are used. (Subroutines PAM1A and PAM2A)

Twelve types of fission reactions may be specified for rigorous calculation. In terms of the input parameter FISSID these are:

U233HE	U235TH
U235HE	U233TH
U235FI	U233FI
U238HE	U238FI
U238TN	P239TH
P239HE	
P239FI	

Here U and P represent uranium and plutonium, the numerical part is the atomic mass and the other symbols represent:

HE	high energy neutron fission
FI	fission spectrum neutron fission
TN	thermonuclear neutron fission
TH	thermal neutron fission

For the non-rigorous, level 3 calculation K factors for the seven most common fission types in the left column are available.

Activity calculations are controlled by the Output Processor Module.

4.2 RIGOROUS ACTIVITY CALCULATION

The following presentation is substantially the same as section 2 of ref. 5; it outlines the operations of the Particle Activity Submodule. It is given in terms of exposure rate, but extension to exposure should be self-evident. Activity from individual nuclides also can be computed by this method. (Subroutine MCHDEP)

4.2.1 Nuclide Abundances

Fission Products

The fission products can be grouped into a number of decay chains, one of which may be represented by

$$N_1 \rightarrow N_2 \rightarrow N_3 \rightarrow \ldots \rightarrow N_m \quad .$$

One or more members (including, of course, N_1) may be produced directly by the fission event, and each member except N_m decays as $e^{-\lambda_i t}$, while each member except N_1 grows by $e^{\lambda_{i-1} t}$. The complete growth and decay history for each member of a chain is represented by the Bateman equation[31]

$$N_n(t) = \sum_{i=1}^{n} \sum_{k=1}^{n} {}_nC_{ki} \, N_i^o \, e^{-\lambda_k t} \quad , \tag{4.2.1}$$

where

$N_n(t)$ = atoms of the nth member of the chain at time t,

N_i^o = atoms of the ith number of the chain ($i \leq n$) at time 0,

and λ_k = disintegration constant of the kth member of the chain ($k \leq n$),

$$ {}_nC_{ki} = \left(\prod_{j=i}^{n-1} \lambda_j \right) \Bigg/ \left(\prod_{\substack{j=i \\ j \neq k}}^{n} (\lambda_j - \lambda_k) \right) \quad . \tag{4.2.2}$$

The activity in disintegrations per second is given by

$$A_n(t) = \lambda_n \, N_n(t) \quad . \tag{4.2.3}$$

The number of disintegrations that occur between times t_1 and t_2 is given by

$$D_n(t_1, t_2) = \lambda_n \sum_{i=1}^{n} \sum_{k=1}^{n} {}_nC_{ki} \, N_i^o \left(e^{-\lambda_k t_1} - e^{-\lambda_k t_2} \right) \Big/ \lambda_k \, , \qquad (4.2.4)$$

which is obtained by integration of eqs. (4.2.1) and (4.2.3). The Bateman equation develops a singularity whenever $\lambda_k = \lambda_{k-1}$. This difficulty is circumvented in DELFIC by slightly incrementing one member of such a pair. (Subroutine BATMAN)

Induced Activity in Soil

The model for the contribution of induced activity in the cloudborne soil was developed by Jones.[32] Three basic assumptions are made:

1. All neutrons entering the soil are thermalized and then captured.
2. Only those neutrons need be considered that are seen by the apparent crater.
3. All significant soil components are refractory in the fractionation scheme.

The model applies only to Nevada Test Site soil. (Subroutine INDCD2)

Induced Activity in Device Materials

The model currently accounts for induced activity in only one device component, ^{238}U. Neutron capture by ^{238}U produces ^{239}U, which decays to ^{239}Np and then ^{239}Pu. The following equations are used:

1. Activity of ^{239}U, dis s^{-1},

$$A_1 = \lambda_1 N_1^o e^{-\lambda_1 t} \, , \qquad (4.2.5)$$

where

N_1^o = number of neutron captures

λ_1 = disintegration constant of ^{239}U, s^{-1},

and t = time, s.

2. Activity of ^{239}Np, dis s^{-1},

$$A_2 = \frac{\lambda_1 \lambda_2 N_1^o}{\lambda_2 - \lambda_1} \left(e^{-\lambda_1 t} - e^{-\lambda_2 t} \right) , \tag{4.2.6}$$

where

λ_2 = disintegration constant of ^{239}Np, s^{-1}.

3. Disintegrations of ^{239}U occurring between t_1 and t_2,

$$\Delta A_1 \Big|_{t_1}^{t_2} = N_1^o \left(e^{-\lambda_1 t_1} - e^{-\lambda_1 t_2} \right) . \tag{4.2.7}$$

4. Disintegrations of ^{239}Np occurring between t_1 and t_2,

$$\Delta A_2 \Big|_{t_1}^{t_2} = \frac{N_1^o}{\lambda_2 - \lambda_1} \left[\lambda_2 \left(e^{-\lambda_1 t_1} - e^{-\lambda_1 t_2} \right) - \lambda_1 \left(e^{-\lambda_2 t_1} - e^{-\lambda_2 t_2} \right) \right] . \tag{4.2.8}$$

5. Disintegrations of ^{239}U from t_1 to infinity,

$$\Delta A_1 \Big|_{t_1}^{\infty} = N_1^o \, e^{-\lambda_1 t_1} \quad . \tag{4.2.9}$$

6. Disintegrations of ^{239}Np from t_1 to infinity,

$$\Delta A_2 \Big|_{t_1}^{\infty} = \frac{N_1^o}{\lambda_2 - \lambda_1} \left(\lambda_2 e^{-\lambda_1 t_1} - \lambda_1 e^{-\lambda_2 t_1} \right) \quad . \tag{4.2.10}$$

This mass chain is considered completely refractory in the fractionation scheme. (Subroutine URAN)

4.2.2 Activity Versus Particle Size

The radial-distribution model of Freiling[33] categorizes a nuclide as volatile if its boiling point is less than the solidification temperature of the soil particles (sec. 2.1.2). The nuclide is refractory if its boiling point is greater than the solidification temperature. Freiling then assumes that a volatile nuclide will condense on the particle surfaces, whereas a refractory nuclide will condense uniformly throughout the particle. A fission-product mass chain, whose composition changes with time, can then be characterized by the fraction of its membership that represents refractory nuclides at the time the cloud cools to the soil-solidification temperature. This Freiling ratio is referred to as F_R. Freiling has postulated, on an empirical basis, that the specific activity of fallout particles is proportional to the $(b_i - 1)$ power of the particle size, where b_i is $\sqrt{F_R}$ for mass chain i.

Freiling[34] has treated the relationship of the model to the log-normal distribution of particle sizes. In DELFIC, however, the model is generalized for arbitrary particle-size distributions. The approach can be formulated as follows:

Let

δ_k = geometric mean diameter of kth particle-size class,

N_k = number of particles in class k,

F_T = total number of equivalent fissions in all size classes,

Y_i = fission yield of ith mass chain,

and r = subscript index for perfectly refractory mass chain.

The equivalent fissions of mass chain i in size class k is

$$F_i(\delta_k) = F_T Y_i f_i(\delta_k) \quad , \tag{4.2.11}$$

where

$$f_i(\delta_k) = N_k \delta_k^{b_i+2} \Big/ \sum_{k=1}^{n} N_k \delta_k^{b_i+2} \tag{4.2.12}$$

For the perfectly refractory chain ($b_i = 1$), Eq. (4.2.11) takes the form

$$F_r(\delta_k) = F_T Y_r f_M(\delta_k) \quad , \tag{4.2.13}$$

where

$$f_M(\delta_k) = N_k \delta_k^3 \Big/ \sum_{k=1}^{n} N_k \delta_k^3 \quad , \tag{4.2.14}$$

i.e., the mass fraction in the kth size class.

The fractionation ratio is given by

$$\left(r_{i,r}\right)_k = \frac{Y_i}{Y_r} \cdot \frac{f_i(\delta_k)}{f_M(\delta_k)} \quad , \tag{4.2.15}$$

or

$$\left(r_{i,r}\right)_k = \frac{Y_i}{Y_r} \cdot \frac{\delta_k^{b_i-1} \sum_{k=1}^{n} N_k \delta_k^3}{\sum_{k=1}^{n} N_k \delta_k^{b_i+2}} \quad . \tag{4.2.16}$$

To obtain an algorithm that takes advantage of the fact that particle size distribution consists of a table of $f_M(\delta_k)$ versus δ_k, we note that

$$\sum_{k=1}^{n} N_k \delta_k^{b_i+2} \Big/ \sum_{k=1}^{n} N_k \delta_k^3 = \sum_{k=1}^{n} \left(f_M(\delta_k)\ \delta_k^{b_i-1}\right) \quad . \tag{4.2.17}$$

Taking

$$E_i = 1 \Big/ \sum_{k=1}^{n} \left(f_M(\delta_k) \cdot \delta_k^{b_i-1}\right) \quad , \tag{4.2.18}$$

we can rewrite eq. (4.2.16)

$$\left(r_{i,r}\right)_k = \frac{Y_i}{Y_r}\ \delta_k^{b_i-1}\ E_i \quad . \tag{4.2.19}$$

It follows from eqs. (4.2.11), (4.2.15) and (4.2.19) that

$$F_i(\delta_k) = F_T Y_i E_i \delta_k^{b_i-1}\ f_M(\delta_k) \quad . \tag{4.2.20}$$

In this form of the radial distribution model, the specific activity for any mass chain that is not perfectly refractory decreases monotonically with increasing particle size. Observations of fallout, on the other hand, provide strong evidence that the specific activity tends to level off at about 100 to 200 μm. To account for this effect, the model was modified in the following manner:

The approach assumes a two-component system. One component obeys the radial distribution model. The other has a constant specific activity over the particle size distribution.

Let

R_i = fraction of fissions in ith mass chain that obeys radial distribution, and

S_i = fraction of fissions in ith mass chain that appears with constant specific activity.

Then Eq. (4.2.20) is replaced by

$$F_i(\delta_k) = F_T Y_i \left(R_i E_i \delta_k^{b_i - 1} + S_i \right) f_M(\delta_k) \quad . \tag{4.2.21}$$

Figure 3, an idealized plot from fallout observations, shows the two components. (Subroutines FRATIO and GXPSR)

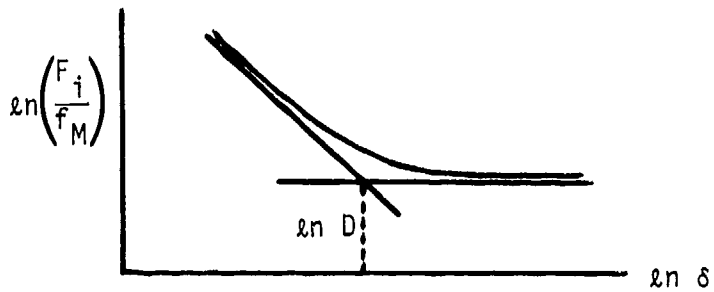

Figure 3. Relationship of equivalent fissions to particle size

The crossing point sets the criterion

$$R_i E_i D^{b_i - 1} = S_i \quad , \tag{4.2.22}$$

since

$$R_i + S_i = 1 \quad , \tag{4.2.23}$$

$$R_i \left(1 + E_i D^{b_i - 1}\right) = 1 \quad , \tag{4.2.24}$$

then

$$R_i = \frac{1}{1 + E_i D^{b_i - 1}} \quad , \tag{4.2.25}$$

and

$$S_i = \frac{E_i D^{b_i - 1}}{1 + E_i D^{b_i - 1}} \quad . \tag{4.2.26}$$

Finally

$$F_i(\delta_k) = \frac{F_T Y_i E_i}{1 + E_i D^{b_i - 1}} \left(\delta_k^{b_i - 1} + D^{b_i - 1}\right) f_M(\delta_k) \quad . \tag{4.2.27}$$

On the basis of fallout observations, D has been taken as 100 μm. (Subroutines FRATIO and GXPSR)

4.3 APPROXIMATE ACTIVITY CALCULATION

For a pure air burst ($\Lambda > 180$ ft $KT^{-1/3.4}$) or for a particle distribution that is specified to be a size-activity distribution, the code performs a conventional calculation in terms of a K factor (Roentgens m^2 KT^{-1} hr^{-1}) and a $t^{-1.26}$ decay factor (t in hours).

If F is the fraction of total cloudborne activity contained in a deposit increment of fallout, the exposure rate or exposure at three feet above one square meter of smooth ground over which the fallout is uniformly spread (Roentgens m^2 hr^{-1} or Roentgens m^2) is

$$A = FW_F K\Phi \qquad (4.3.1)$$

where W_F is total fission yield (KT), and for exposure rate

$$\Phi = t^{-1.26}$$

while for exposure from t_1 to t_2

$$\Phi = (t_1^{-0.26} - t_2^{-0.26})/0.26 \quad .$$

(Subroutines PAM1A, PAM2A and PCHECK)

4.4 HEIGHT-OF-BURST EFFECT

For scaled heights of burst in the range $0 < \Lambda < 180$ (ft $KT^{-1/3.4}$) there is at present not a satisfactory means available to compute the cloudborne

particle size distribution nor to distribute activity over this distribution. Complex calculations would be required to develop the information required and this work has not been done.

DELFIC uses a very rough procedure to correct for height of burst. This makes use of empirical data that relate fraction of total activity observed in local fallout to scaled height of burst.[35] In terms of the fraction of local surface burst activity observed, f_d, Showers[36] has expressed these data in the form

$$f_d = (0.45345)^{\lambda/65} \quad ; 0 < \lambda \tag{4.4.1}$$

where λ is scaled height of burst in terms of ft $KT^{-1/3}$. The fission yield is simply scaled down by this factor to correct for height of burst. Of course, if $\Lambda \geq 180$ (ft $KT^{-1/3.4}$), we assume that no local fallout occurs, and the pure air burst mode of calculation proceeds. (Subroutine OPM1)

5. MAP PREPARATION

5.1 GENERAL DISCUSSION

In this chapter we discuss the operations of the Output Processor Module (OPM). The OPM receives fallout deposit increment descriptions from the Diffusive Transport Module and processes them into fallout maps specified by the user. Activity calculations are performed as required for the requested maps. The maps are printed by a standard line printer. A printed and punched card output also can be prepared which consists of coordinates of points on specified contours in the maps.

Eighteen map types (Table 1), of which sixteen are unique, may be requested. All but three of these are available for any of the three levels of activity calculation (sec. 4.1); the exceptions being options 9, 10 and 14 which are available only via the completely rigorous calculation.

5.2 DEPOSIT INCREMENT PROCESSING

In sec. 3.4 above we discuss how an individual deposit increment (i.e., a ground impacted fallout parcel) is described in terms of its impact point coordinates, x_p, y_p, orientation axis of the standard deviation ellipse, α, downwind and crosswind standard deviations, $\sigma_{\parallel}$, $\sigma_{\perp}$, along with other properties such as particle diameter and mass. (See Figs. 2 and 4.) These quantities are unique for each deposit increment and it is the principle task of the OPM to compute and sum contributions from all deposit increments at each map point.

Consider a deposit increment with area integrated activity or total mass Q. Then at a point x,y, the activity or areal density of mass $\omega(x,y)$, is

$$\omega(x,y) = \frac{Q}{2\pi\sigma_{\parallel}\sigma_{\perp}} \exp\left[-\frac{(X-X_p)^2}{2\sigma_{\parallel}^2} - \frac{(Y-Y_p)^2}{2\sigma_{\perp}^2}\right] \qquad (5.2.1)$$

TABLE 1

MAP REQUEST OPTIONS

Map Option Code, NREQ	Description
0	Termination of request set.
1	Count of fallout deposit increments that contribute to each map ordinate.
2	Exposure rate normalized* to H + 1 hour (Roentgen hr^{-1}).
3	Exposure rate at time H + T1 hours, accounting for time of arrival of fallout. (Roentgen hr^{-1})
4	H + 1 hour normalized* exposure rate resulting from particles in diameter range T1 to T2 micrometers.** (Roentgen hr^{-1}).
5	Integrated exposure from H + T1 hours to infinity, accounting for time of arrival of fallout by the approximate method.+ (Roentgen).
6	Integrated exposure from H + T1 to H + T2 hours, accounting for time of arrival of fallout by the approximate method.+ (Roentgen)
7	Integrated exposure from H + T1 to H + T2 hours assuming all fallout has arrived by H + T1 hours. (Roentgen).
8	Integrated exposure from H + T1 hours to infinity assuming all fallout has arrived by H + T1 hours. (Roentgen).
9	Integrated exposure from H + T1 hours to infinity, accounting for time of arrival of fallout by the exact method.++ (Roentgen)
10	Integrated exposure from H + T1 to H + T2 hours, accounting for time of arrival of fallout by the exact method.++ (Roentgen).
11	Mass of fallout per unit area (kg m^{-3}).

TABLE 1 (con't.)

Map Option Code, NREQ	Description
12	Mass of fallout per unit area deposited from H + T1 to H + T2 hours (kg m^{-3}).
13	Mass of fallout per unit area deposited by particles in diameter range T1 to T2 micrometers.** (kg m^{-3})
14	Activity per unit area from an individual mass chain at T1 hours in units of curies m^{-2}, or in equivalent fissions m^{-2} if T1 = 0.
15	Time of onset of fallout. (s)
16	Time of cession of fallout. (s)
17	Diameter of smallest particle deposited. (μm)
18	Diameter of largest particle deposited. (μm)

---

* A "normalized" calculation is one in which it is assumed that all fallout is deposited by H + t regardless of actual deposition time.

** When specifying T1 and T2 particle diameters, make T1 slightly smaller and T2 slightly larger than the tabulated central diameters for the particle size classes.

\+ The $t^{-1.26}$ decay factor is used to compute exposure rate at times other than H + 1 hour (sec. 4.3), though activity at H + 1 hour may be calculated by the rigorous method. (See sec. 4.1)

++ Warning: This calculation probably will consume a lot of computer time. A complete activity calculation is done for each deposit increment of fallout. Consider using one of the approximate methods (requests 5 and 6).

where

$$X = x\cos\alpha + y\sin\alpha$$

$$Y = y\cos\alpha - x\sin\alpha \qquad (5.2.2)$$

and X_p and Y_p are defined similarly. The x,y, and X,Y coordinate axes are related as shown in Fig. 4.

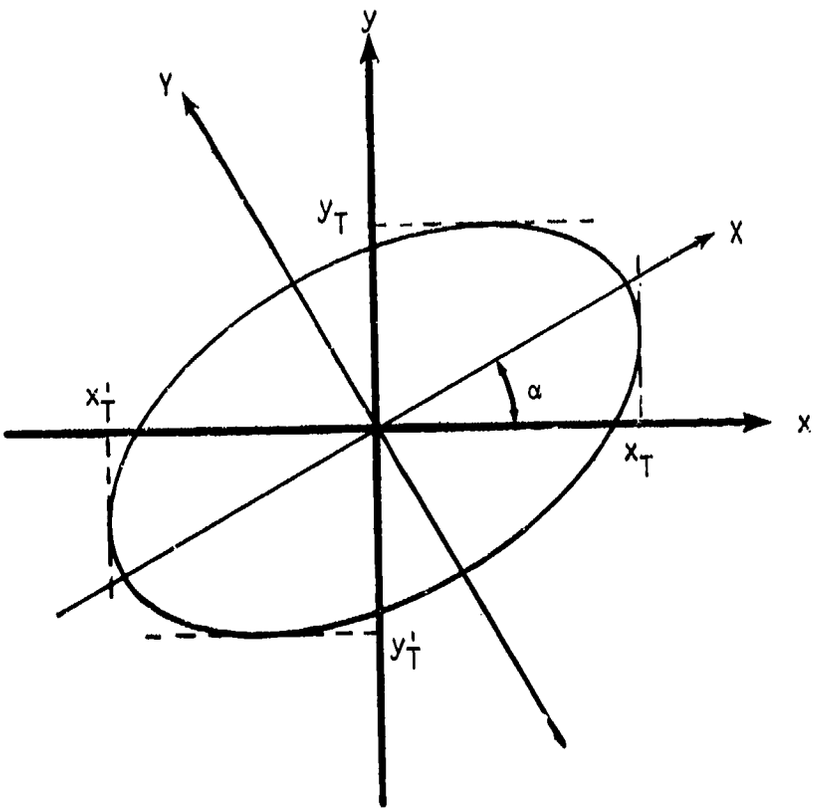

Figure 4. A deposit increment concentration ellipse in the x,y plane.

A parameter ω_{min}, specified by the user or calculated by the program, (II, Appendix B), is defined which represents the lower threshold value for contributions from individual deposit increments; that is, any $\omega(x,y) < \omega_{min}$ is ignored. To determine the elliptical envelope within which $\omega(x,y) \geq \omega_{min}$, we define a quantity γ

$$\gamma = \ell n \left(\frac{Q}{2\pi\sigma_{\parallel}\,\sigma_{\perp}\,\omega_{min}} \right) \; ; \quad \gamma > 0 \quad . \tag{5.2.3}$$

From eq. (5.2.1) it is apparent that

$$\gamma = \frac{(X-X_p)^2}{2\sigma_{\parallel}^{\,2}} + \frac{(Y-Y_p)^2}{2\sigma_{\perp}^{\,2}} \quad , \tag{5.2.4}$$

which is the equation of the desired ellipse.

Figure 4 shows such an ellipse with tangent lines drawn parallel with the x,y axes and cutting these axes at points x_T, x_T', y_T, y_T'. From the general properties of an ellipse, it can be shown that these lines are

$$x_T, x_T' = x_p \pm \sqrt{2\gamma\,(\sigma_{\parallel}^2 \cos^2\alpha + \sigma_{\perp}^2 \sin^2\alpha)} \quad , \tag{5.2.5}$$

and

$$y_T, y_T' = y_p \pm \sqrt{2\gamma\,(\sigma_{\parallel}^2 \sin^2\alpha + \sigma_{\perp}^2 \cos^2\alpha)} \; . \tag{5.2.6}$$

In the code, computation of x_T, x_T' and y_T, y_T' is used to establish whether or not a deposit increment contributes to a particular map or map section.

For each deposit increment, map points are considered row-by-row. The bounding rows are determined from the y_T, y_T' values. For a particular row, the bounding x coordinates, x_c, x_c', are given by

$$x_c, x_c' = x_p + \frac{(y-y_p)\left(\frac{1}{\sigma_\perp^2} - \frac{1}{\sigma_{\shortparallel}^2}\right)\sin\alpha\cos\alpha \pm \sqrt{-\left(\frac{y-y_p}{\sigma_{\shortparallel}\sigma_\perp}\right)^2 + 2\gamma\left(\frac{\cos^2\alpha}{\sigma_{\shortparallel}^2} + \frac{\sin^2\alpha}{\sigma_\perp^2}\right)}}{\frac{\cos^2\alpha}{\sigma_{\shortparallel}^2} + \frac{\sin^2\alpha}{\sigma_\perp^2}} \qquad (5.2.7)$$

In preparing maps for time of onset or cessation of fallout, or largest or smallest particle, the procedure above is applied with ω_{min} for mass per unit area of fallout.

6. VALIDATION

6.1 DISCUSSION

Predictions are compared with observed H + 1 hour normalized* exposure rate maps for the five test shots described in Table 2. The predictions were executed as discussed in reference 38, using the data listed there. Observed fallout patterns were taken from DASA 1251.

Three methods of comparison of fallout patterns are used here:

1. Visual comparison of contour maps.
2. Comparison of contour areas, and hotline lengths and azimuths.**
3. The Rowland-Thompson Figure-of-Merit (FM).[39] (Appendix C)

These are roughly in order of importance.

Statistical data are in Table 3 and the contour plots are on pp. 64 through 73. The contours were drawn by a 30-inch Calcomp plotter, and each observed-predicted pair are to the same scale.

TABLE 2

TEST SHOT DATA

Shot	Total Yield (KT)	Fission Yield (KT)	HOB (m)	Altitude of GZ (m)	Site
Johnie Boy	0.5	0.5	-0.584	1570.6	NTS+
Jangle-S	1.2	1.2	1.067	1284.7	NTS
Small Boy	low	-	3.048	938.2	NTS
Koon	150.	-	4.145	0.0	Bikini
Zuni	3380.	-	2.743	0.0	Bikini

+Nevada Test Site

*A "normalized" exposure rate map is constructed on the assumption that all local fallout is down at the specified time, regardless of its actual deposition time.

**Hotline length is defined as the furthest distance from ground zero on a contour, and hotline azimuth is the angle, measured clockwise from north, to the point of furthest distance from ground zero on a contour.

TABLE 3

COMPARISON OF OBSERVED AND PREDICTED FALLOUT PATTERN STATISTICS

Observed/Predicted

Test Shot	FM	Contour (Roentgen hr^{-1})	Area (km^2)	Hotline Length(km)	Azimuth (deg)
Johnie Boy	0.182	1000	0.278/0.029	1.38/0.32	359/0
		100	0.539/0.774	2.73/2.58	345/344
		50	1.271/1.787	4.10/4.13	343/343
			58(42)*	28(3)*	
Jangle-S	0.483	500	0.117/0.144	0.59/1.00	342/353
		300	0.386/0.316	1.50/1.23	346/354
		100	1.437/2.242	3.74/5.87	1/355
		35	3.114/5.077	5.06/7.68	6/355
			40(45)	43(42)	
Small Boy	0.308	1000	0.216/0.047	1.00/0.25	71/66
		500	0.528/0.135	1.62/0.56	73/80
		200	0.942/0.564	2.22/1.69	72/73
		100	3.75/1.10	5.66/3.72	72/74
		50	9.03/4.38	8.10/6.47	75/72
			63(59)	44(36)	
Koon	0.287	500	32.0/26.0	10.2 /12.5	18/0
		250	122/87.3	17.3 /24.2	15/4
		100	550/261	41.0 /39.5	17/3
			33(40)	22(22)	
Zuni	0.105	150	474/2239	98/78	12/337
		100	2761/3619	125/96	17/337
		50	6187/6660	138/121	27/338
		30	10950/9913	177/153	33/340
			105(16)	17(16)	

*Mean absolute percent errors. The value in parentheses is calculated without including the data for the highest activity level contour. See footnote next page.

Prediction accuracy is seen to be good, particularly for the low yield shots. Overall mean absolute percent errors* for contour area and hotline length are 61 and 32 percent respectively. If the data for the highest activity level contours are excluded, we have 42 and 26 percent for these errors. The highest level contours are particularly difficult to predict, usually being in the region affected by throwout and induced activity in and around the crater. DELFIC does not address this portion of the activity field since fallout is a negligible contributor to casualities there.

It is important to emphasize that this level of prediction competency is achieved without a posteriori adjustment or calibration of any aspect of the model such as to improve agreement with any observed fallout pattern.

The three low yield shots were executed at the Nevada Test Site, and their fallout patterns were measured over land. For this reason, observed patterns for these shots, though not highly accurate, may be considered to be superior to the patterns of the high yield shots which were executed on Bikini Atoll in the South Pacific. Not only are the fallout fields of the high yield shots very large, which adds to measurement problems, but most of the fallout from these shots fell into water. Even so, most of the Koon pattern area was covered by an array of fallout collection stations, so this pattern is probably reasonably accurate. Zuni, on the other hand, is a special case. The fallout pattern used here is exclusively downwind of the atoll and was determined by an oceanographic survey method that was known to be inaccurate. The close-in pattern in the region of the atoll is available, but contains no closed contours so could not be used here; thus the high-activity portion of the observed pattern for this shot is ignored, and this alone must account for a substantial portion of the disagreement

*For n observed-predicted data pairs, mean absolute percent error is

$$\frac{100}{n} \sum_{i=1}^{n} \left| x_{obs,i} - x_{pred,i} \right| / x_{obs,i} \quad .$$

between observation and prediction for this shot, particularly with regard to contour areas and overlap (Table 3). In addition, we have the following problem.

Predictions for these high yield shots are expected to be inferior to those for these low yield shots. This is because both of the high yield shots were detonated over coral soil, and in the case of Zuni, a large but uncertain amount of sea water was lifted by the cloud. The particle size distribution used for these predictions is typical of fallout produced from the siliceous soil found at the Nevada Test Site. We have not succeeded in developing a distribution appropriate for coral and coral-sea water mixtures.

More details concerning the prediction calculations and test shot characteristics are in reference 38.

6.2 OBSERVED AND PREDICTED FALLOUT PATTERNS

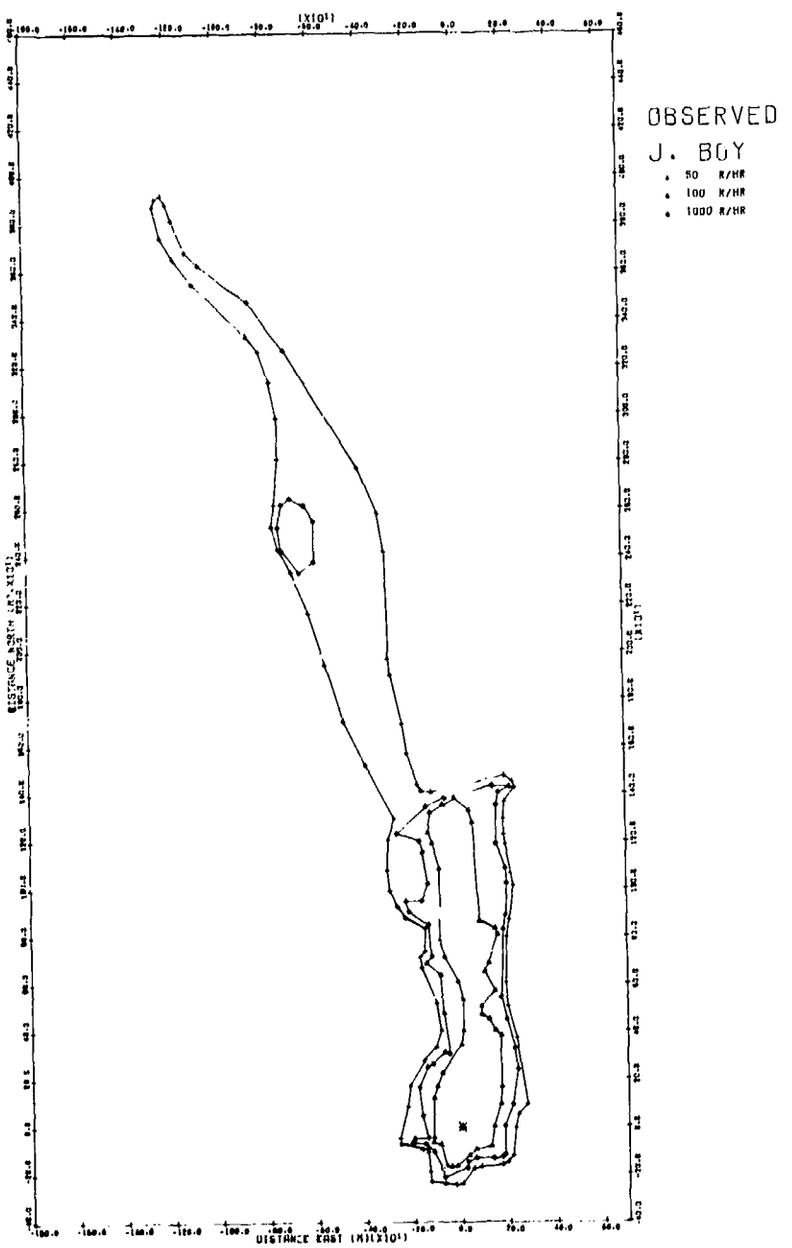

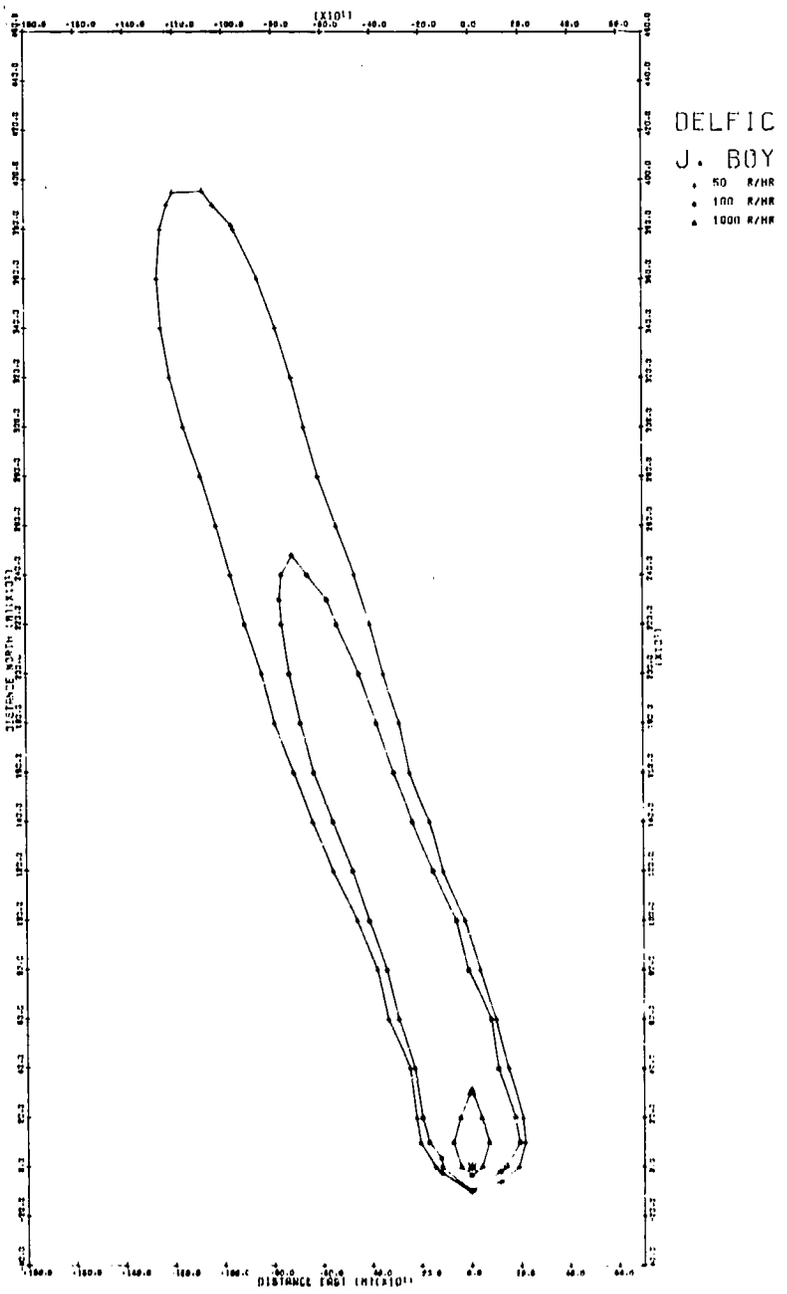
DELFIC
J. BOY
50 R/HR
100 R/HR
1000 R/HR

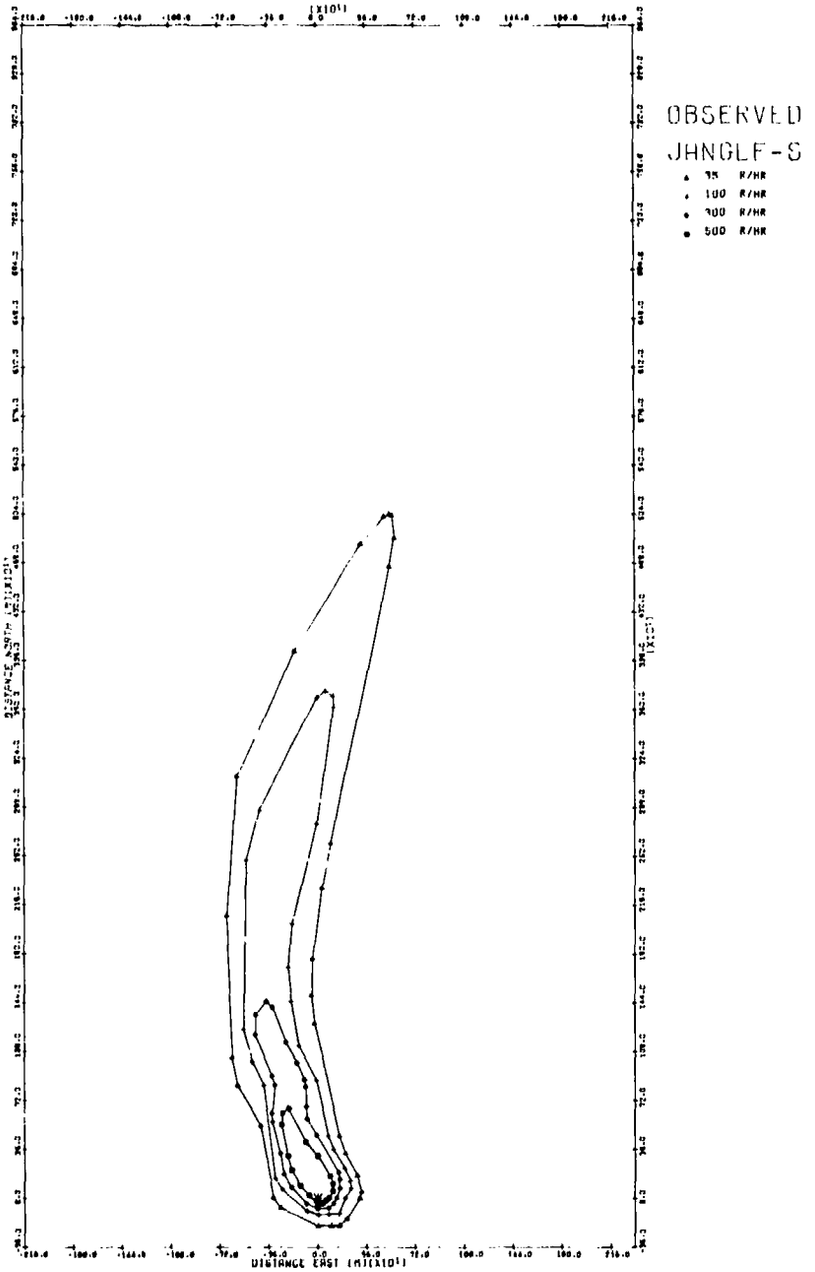
OBSERVED
JHNGLE-S
▲ 25 R/HR
• 100 R/HR
• 300 R/HR
● 500 R/HR
DISTANCE EAST (FT)(X10¹)

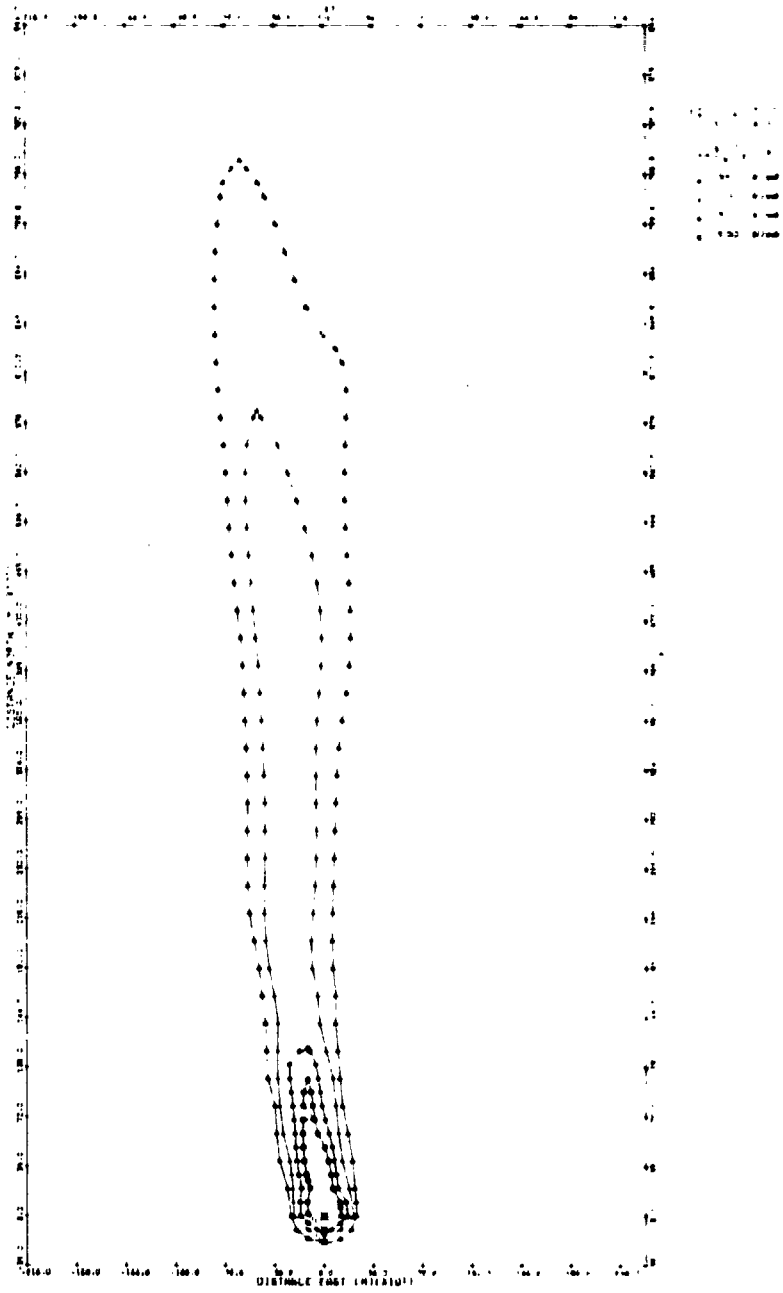

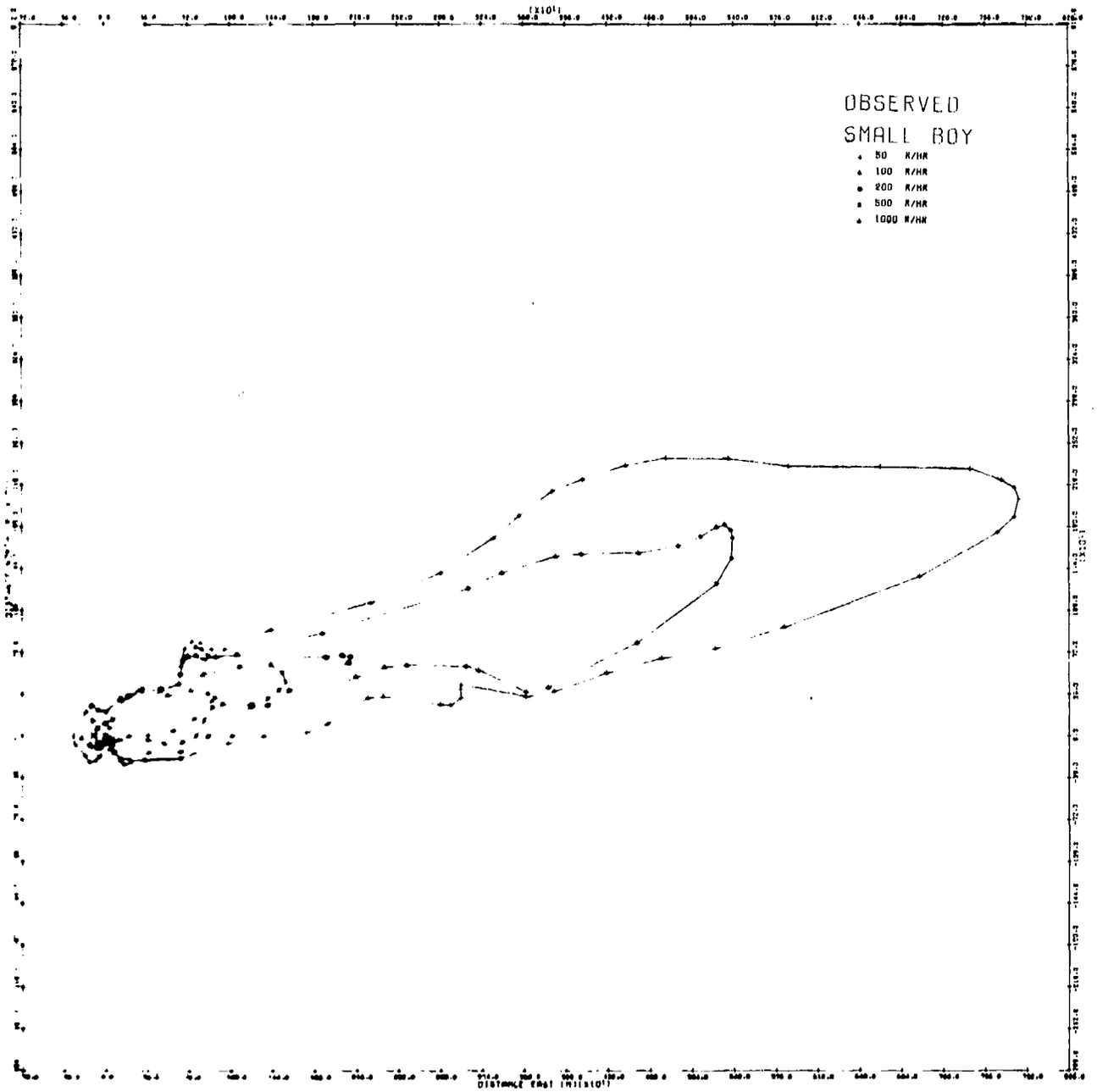
OBSERVED
SMALL BOY
50 R/HR
100 R/HR
200 R/HR
500 R/HR
1000 R/HR

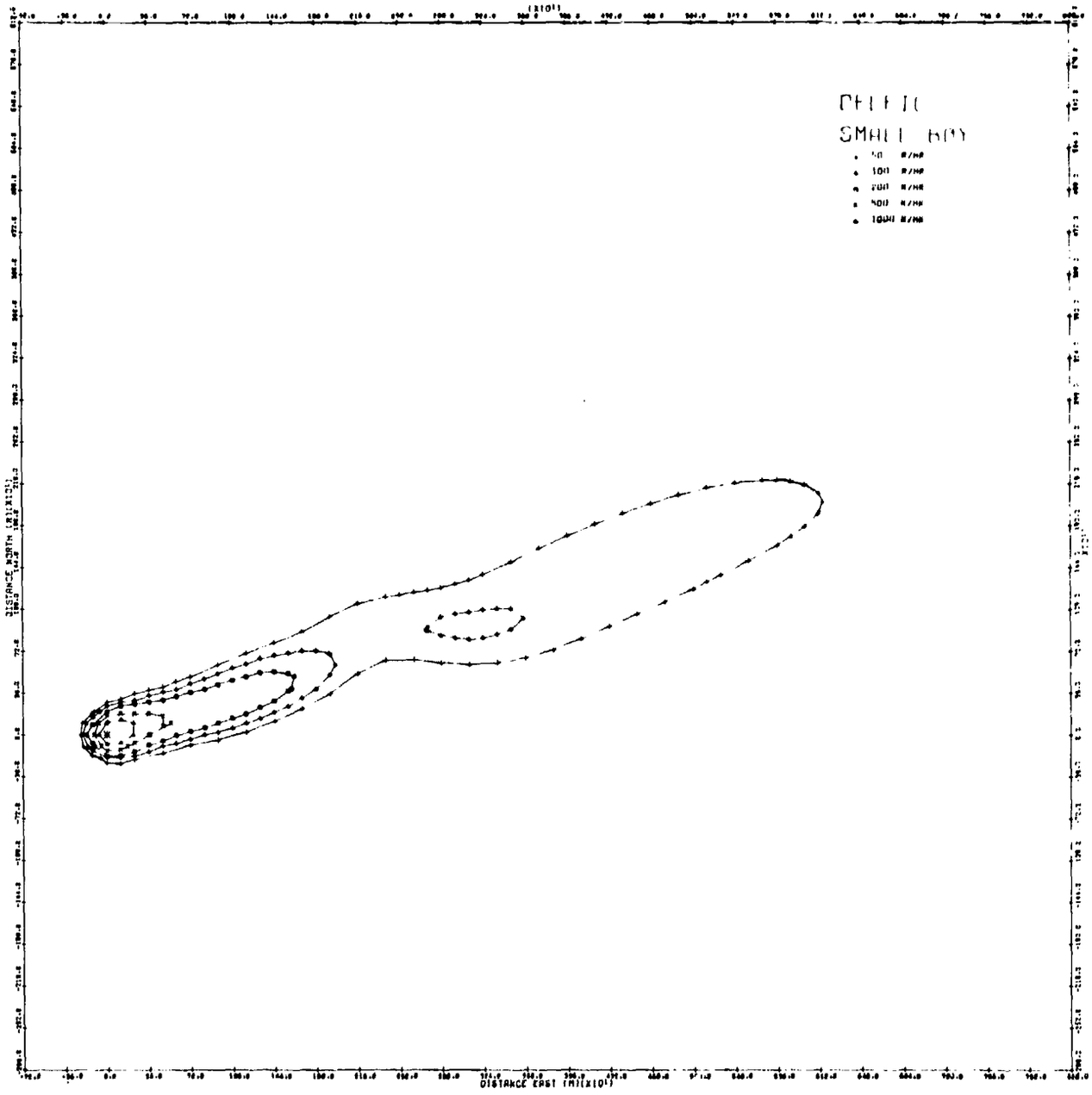
SMALL BOY
DISTANCE EAST (MI)(X10¹)

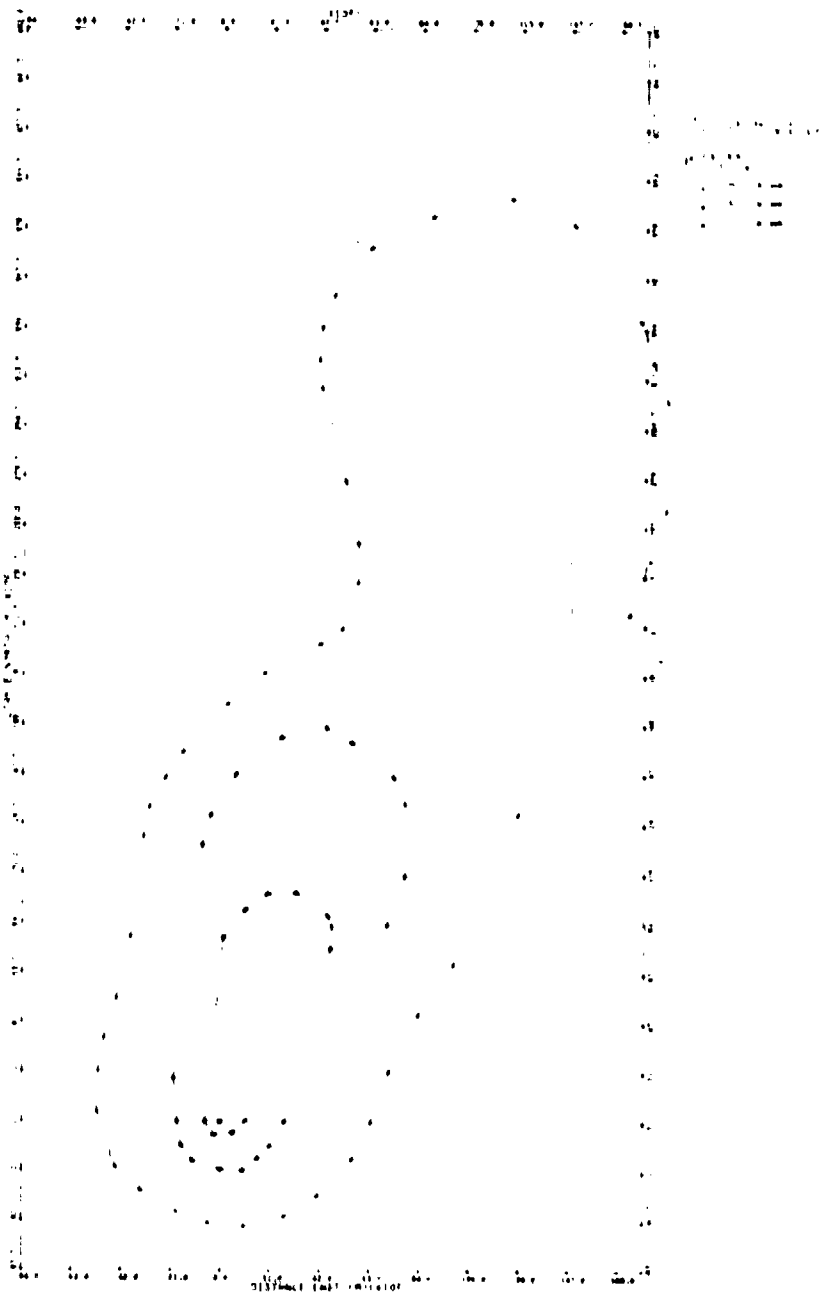

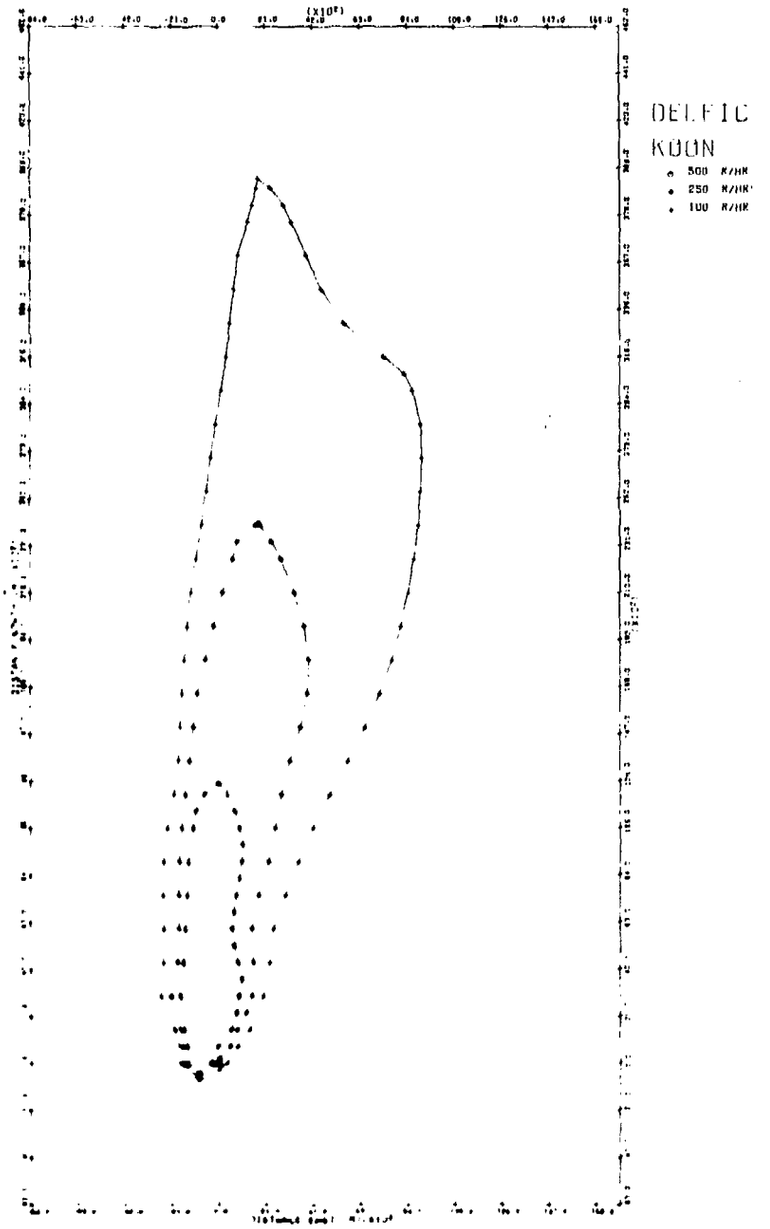
DELFIC
KOON
500 R/HR
250 R/HR
100 R/HR

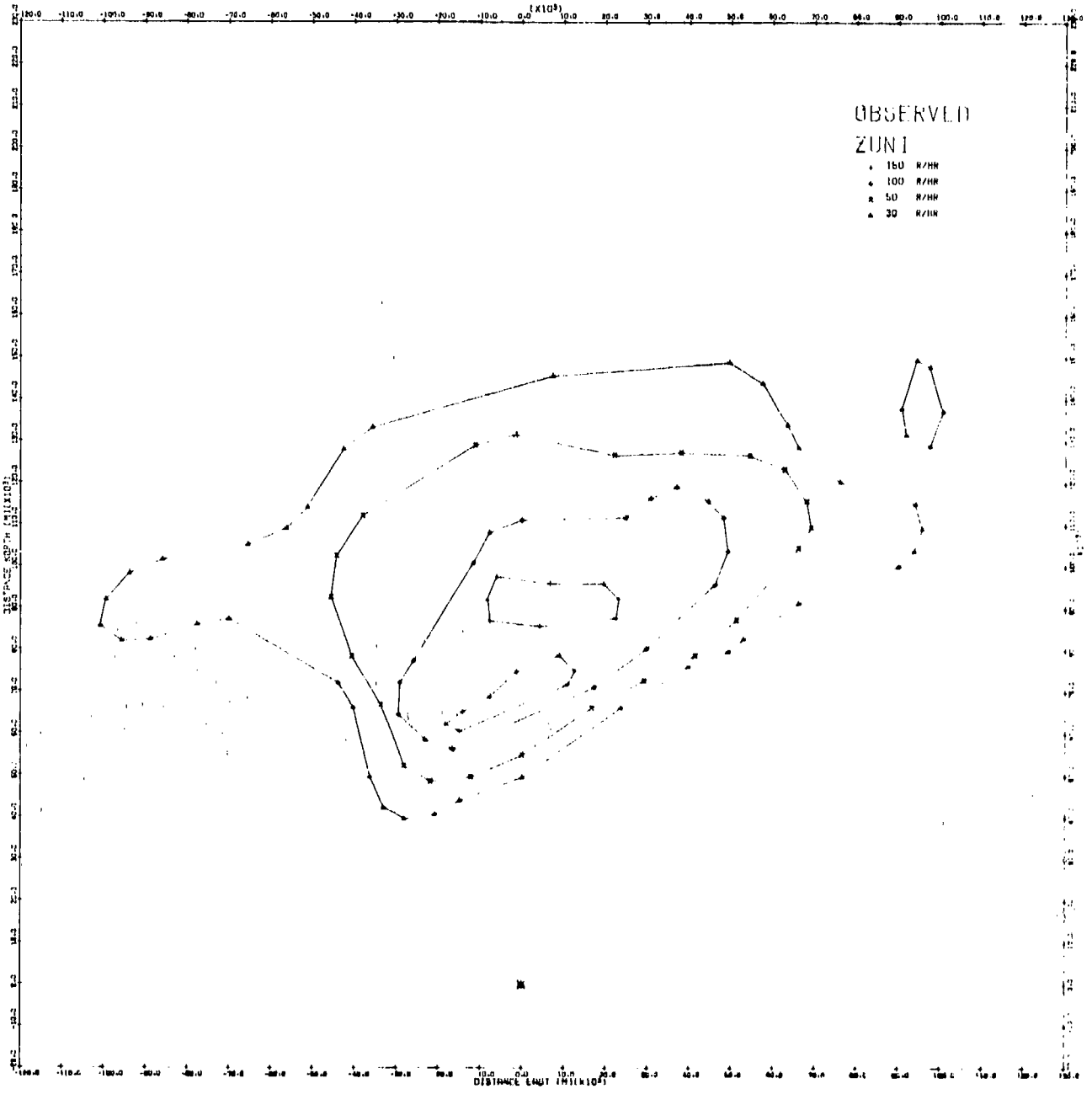
OBSERVED
ZUNI
150 R/HR
100 R/HR
50 R/HR
30 R/HR
DISTANCE EAST (MILES X10³)
DISTANCE SOUTH (MILES X10³)

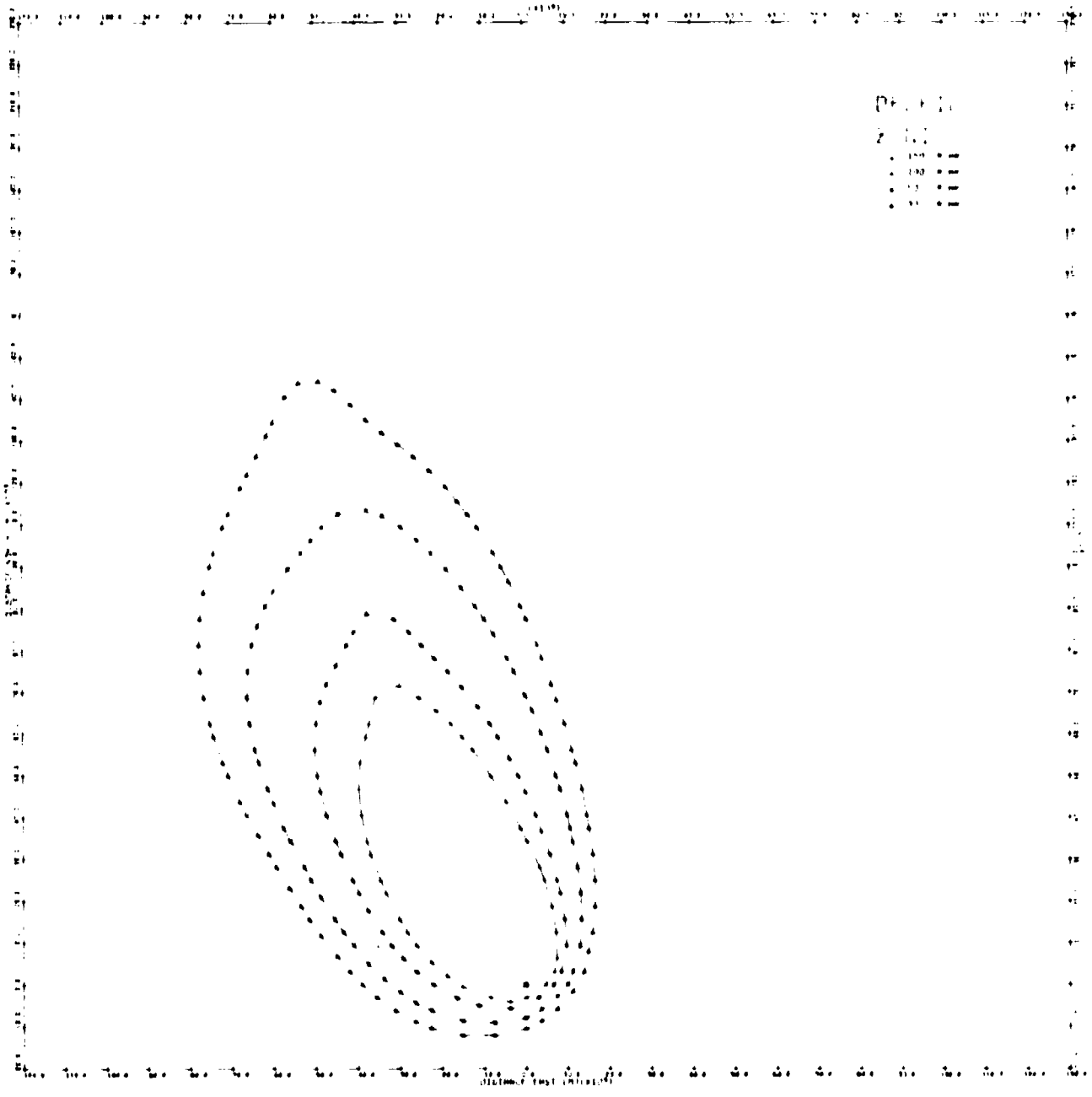

REFERENCES

1. H. G. Norment, "Department of Defense Land Fallout Prediction System, Volume I. System Description," Technical Operations Research, TO-B 66-40, DASA 1800-I (27 June 1966). AD- 483 897.

2. H. G. Norment, W.Y.G. Ing and J. Zuckerman, "Department of Defense Land Fallout Prediction System. Volume II. Initial Conditions," Technical Operations Research, TO-B 66-44, DASA 1800-II (30 September 1966). AD-803 144.

3. I. O. Huebsch, S. H. Cassidy, H. G. Norment, J. Zuckerman, and T. W. Schwenke, "Department of Defense Land Fallout Prediction System. Volume III, Cloud Rise," TO-B 66-45, DASA-1800-III (19 May 1967). AD-819 770.

4. H. G. Norment, T. W. Schwenke, I. Kohlberg and W.Y.G. Ing, "Department of Defense Land Fallout Prediction System. Volume IV. Atmospheric Transport," Technical Operations Research, TO-B 66-46, DASA-1800-IV, (2 February 1967). AD-815 263

5. R. C. Tompkins, "Department of Defense Land Fallout Prediction System, Volume V. Particle Activity," NDL-TR-102, DASA-1800-V (February 1968). AD-832 239.

6. T. W. Schwenke and P. Flusser, "Department of Defense Land Fallout Prediction System. Volume VI. Output Processor," TO-B 66-48, DASA-1800-VI (20 February 1967). AD-814 055.

7. D. K. Winegardner, "Department of Defense Land Fallout Prediction System, Volume VII. Operators' Manual," NDL-TR-104, DASA-1800-VII (April 1968). AD-836 871.

8. H. G. Norment and S. Woolf, "Department of Defense Land Fallout Prediction System, Volume III (Revised)," R70-1W. DASA-1800-III (Revised) (1 September 1970). AD-879 890.

9. H. G. Norment, "Department of Defense Land Fallout Prediction System, Volume II, Initial Conditions," DNA 1800-II (Supplement), (October 1972). AD-753 842.

10. H. G. Norment and E. J. Tichovolsky, "A New Fallout Transport Code for the DELFIC System: The Diffusive Transport Module." Arcon Corporation, R71-W, DASA-2669 (1 March 1971). AD-727 613. H. G. Norment, Mt. Auburn Research Associates, DNA-2669 - Supplement (October 1972). AD-751 542.

11. H. G. Norment, "A Revised Output Processor Module for the DELFIC Fallout Prediction System," DNA 2962F (October 1972). AD-751 543.

12. H. G. Norment, "A Precipitation Scavenging Model for Studies of Tactical Nuclear Operations. Vol. I: Theory and Preliminary Results. Vol. II: The DELFIC-PSM Code," DNA-3661F-1 and DNA-3661F-2 (May 1975) AD-014 960/9GI and AD-014 961/7GI.

13. H. G. Norment, "Validation and Refinement of the DELFIC Cloud Rise Module," Atmospheric Science Associates, DNA-4320F (15 January 1977) AD-A047 372.

14. M. D. Nordyke, "On Cratering: A Brief History, Analysis, and Theory of Cratering," Lawrence Radiation Laboratory, UCRL-6578 (22 August 1961).

15. H. G. Norment and W. Woolf, "Studies of Nuclear Cloud Rise and Growth," Technical Operations, Inc., unpublished.

16. I. O. Huebsch, "The Development of a Water-Surface-Burst Fallout Model: The Rise and Expansion of the Atomic Cloud," USNRDL-TR-741 (23 April 1964). AD-441 983.

17. I. O. Huebsch, "Turbulence, Toroidal Circulation and Dispersion of Fallout Particles from the Rising Nuclear Cloud," USNRDL-TR-1054 (5 August 1966).

18. K. V. Beard, "Terminal Velocity and Shape of Cloud and Precipitation Drops Aloft," J. Atm. Sci. 33, 851 (1976).

19. C. N. Davies, "Definitive Equations for the Fluid Resistance of Spheres," Proc. Phys. Soc. (London) 57, 259 (1945).

20. J. Aitchison and J.A.C. Brown, The Lognormal Distribution (Cambridge University Press, 1966).

21. M. W. Nathans, R. Thews, W. D. Holland and P. A. Benson, "Particle Size Distribution in Clouds from Nuclear Airbursts," J. Geophys. Res. 75, 7559 (1970).

22. E. C. Freiling, "A Comparison of the Fallout Mass-Size Distributions Calculated by Lognormal and Power-Law Models," USNRDL-TR-1105, U. S. Naval Radiological Defense Laboratory (14 November 1966). AD-646 019.

23. J. J. Walton, "Scale Dependent Diffusion," J. Appl. Meteor. 12, 547 (1973).

24. G. T. Csanady, "Turbulent Diffusion of Heavy Particles in the Atmosphere," J. Atm. Sci. 20, 201 (1963).

25. W. Y. Chen, "Energy Dissipation Rates in Free Atmospheric Turbulence," J. Atm. Sci. 31, 2222 (1974).

26. E. M. Wilkins, "Decay Rates for Turbulent Energy Throughout the Atmosphere," J. Atm. Sci. 20, 473 (1963).

27. E. H. Barker and T. L. Baxter, "A Note on the Computation of Atmospheric Surface Layer Fluxes for Use in Numerical Modeling," J. Appl. Meteor. 14, 620 (1975).

28. F. Pasquill, Atmospheric Diffusion, 2nd edition (Halsted Press, 1974).

29. D. Golder, "Relations Among Stability Parameters in the Surface Layer," Boundary-Layer Meteor. 3, 47 (1972).

30. G. P. Cressman, "An Operational Objective Analysis System," Monthly Weather Review 87, 367 (1959).

31. H. Bateman, "The Solution of a System of Differential Equations Occuring in the Theory of Radioactive Transformations," Proc. Cam. Phil. Soc. 15, 423 (1910).

32. T. H. Jones, "A Prediction System for the Neutron-Induced Activity Contribution to Fallout Exposure Rates," USNRDL-TR-1056, U.S. Naval Radiological Defense Laboratory (1966).

33. E. C. Freiling, "Fractionation I. High-Yield Surface Burst Correlation," USNRDL-TR-385, U.S. Naval Radiological Defense Laboratory (29 October 1959). AD-232 085.

34. E. C. Freiling, "Fractionation III. Estimation of Degree of Fractionation and Radionuclide Partition for Nuclear Debris," USNRDL-TR-680, U.S. Naval Radiological Defense Laboratory (September 1963). AD-423 725.

35. P. D. LaRiviere, et al., "Local Fallout From Nuclear Test Detonations. Vol. V. Transport and Distribution of Local (Early) Fallout From Nuclear Weapons Tests," unpublished.

36. R. L. Showers, "Improvements to the PROFET Fallout Prediction Program," Ballistics Research Laboratories, BRL-MR-2095 (February 1971). AD-883 280.

37. M. Abramowitz and I. A. Stegun, Handbook of Mathematical Functions, NBS-AMS 55 (June 1964).

38. H. G. Norment, "Evaluation of Three Fallout Prediction Models: DELFIC, SEER and WSEG-10," Atmospheric Science Associates, DNA 5285F (16 June 1978).

39. R. H. Rowland and J. H. Thompson, "A Method for Comparing Fallout Patterns," DASIAC, G. E. - Tempo. DNA 2919F (April 1972).

APPENDIX A

THE LOGNORMAL DISTRIBUTION

FUNDAMENTALS

A variable x is said to be normally distributed if the probability of its occurrence in the range x to x + dx is given by

$$dN(x|\mu,\sigma^2) = \frac{1}{\sigma\sqrt{2\pi}} \exp\left[-\frac{1}{2}\left(\frac{x-\mu}{\sigma}\right)^2\right] dx, \qquad (A.1)$$

where μ is the mean value of x and σ^2 is the variance of x. The square root of the variance, σ, is called the standard deviation.

To define a lognormal distribution, we make the transformation

$$x = \ell n(y) \quad . \qquad (A.2)$$

In terms of the variable y eq. (A.1) becomes

$$d\P(y|\mu,\sigma^2) = \frac{1}{\sigma\sqrt{2\pi}} \exp\left[-\frac{1}{2}\left(\frac{\ell ny-\mu}{\sigma}\right)^2\right] d(\ell ny) \quad , \qquad (A.3)$$

and y is said to be lognormally distributed.[20]

Some statistical properties of y are as follows:

$$\text{mean}(y) = \exp\left(\mu + \frac{1}{2}\sigma^2\right) \qquad (A.4)$$

$$\text{median}(y) = \exp(\mu) \qquad (A.5)$$

$$\text{mode}(y) = \exp(\mu - \sigma^2) \tag{A.6}$$

$$\text{variance}(y) = \left[\exp(\sigma^2) - 1\right] \exp(2\mu + \sigma^2). \tag{A.7}$$

Let $\underset{\sim}{y}$ and s be the geometric mean and geometric standard deviation of y. Then

$$\underset{\sim}{y} = \text{median}(y) = \exp(\mu) \tag{A.8}$$

and

$$s = \exp(\sigma) \ . \tag{A.9}$$

Let λ_j' be the j-th moment of $\pi(y|\mu,\sigma^2)$ about the origin. Then by definition

$$\lambda_j' = \int_0^\infty y^j \, d\pi(y|\mu,\sigma^2) \ , \tag{A.10}$$

and from the properties of the normal distribution it follows that

$$\lambda_j' = \exp(j\mu + \tfrac{1}{2} j^2\sigma^2) \ . \tag{A.11}$$

A feature that distinguishes the lognormal distribution from the normal distribution is the existance of moment distributions. The j-th moment distribution is defined as

$$\pi(y|\mu,\sigma^2)_j = \frac{1}{\lambda_j'} \int_0^y t^j d\pi(t|\mu,\sigma^2) \ , \tag{A.12}$$

which can be shown to be[20]

$$\P(y|\mu,\sigma^2)_j = \P(y|\mu + j\sigma^2,\sigma^2) \quad . \tag{A.13}$$

The moment distributions provide simple relationships between lognormal distributions of number, surface area, and volume of particles with respect to their diameters.

APPLICATION TO PARTICLE DISTRIBUTIONS

In discussions of lognormal particle distributions, confusion frequently arises because distinction is not clearly made between μ and $\underline{y}$ and between σ and s. Since numerical values of μ and σ depend on the base of the logarithms used, we confine our discussion to $\underline{y}$ and s.

Suppose we have plotted cumulative numbers of particles versus diameter on log-probability graph paper and have obtained the curve shown in Fig. A.1. This straight-line curve indicates that the distribution of particle number with respect to diameter, δ, is lognormal. Thus, δ is equivalent to y in eq. (A.3) and from eqs. (A.8) and (A.9) we have

$$\underline{y} = \delta_{50}$$

and

$$s = \delta_{84.13}/\delta_{50} \text{ or } s = \delta_{50}/\delta_{15.87} \quad .$$

These are the quantities DMEAN (μm) and SD (dimensionless), respectively, that are required as input to subroutine ICM. (DMEAN is the median particle diameter in the distribution of numbers of particles with respect to their diameters.)

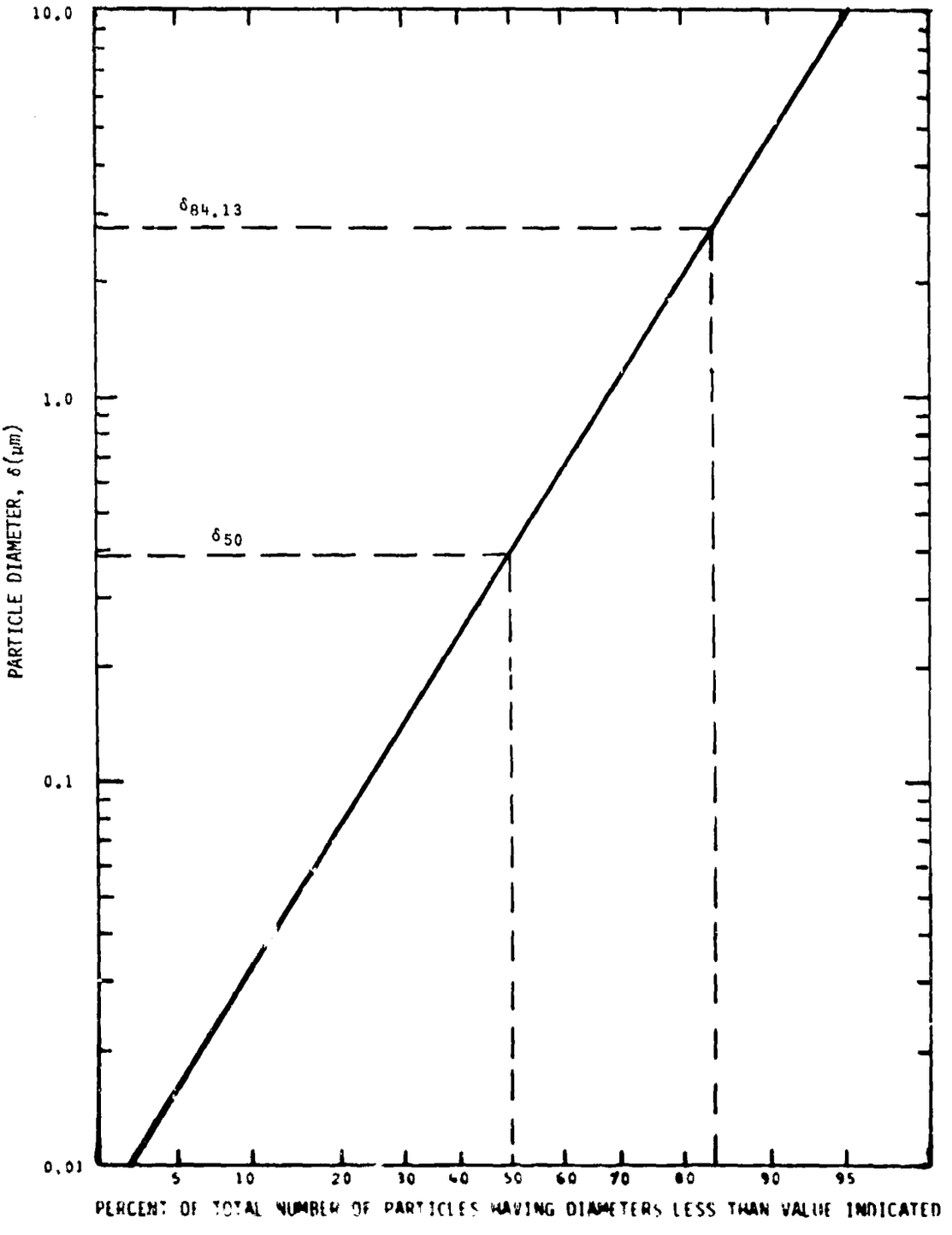

Figure A.1 Cumulative frequency graph of lognormally distributed particles

As noted above, the properties of the moment distributions are useful in interrelating distributions of particle number, surface area, and volume with respect to particle diameter. This is because the number distribution is the zeroth moment distribution with respect to diameter, surface area is distributed via the second moment distribution, and volume is distributed via the third moment distribution. Thus, if we assume spherical particles and if the parameters μ and σ are known for either the particle number, or particle area, or particle volume distribution with diameter, then the other distributions can be determined from the equations below. The parameter σ is the same for all three distributions. If we use N, S, and V as subscripts to denote number, surface area, and volume, respectively, we have from eq. (A.13)

$$\mu_S = \mu_N + 2\sigma^2$$

$$\mu_V = \mu_N + 3\sigma^2$$

where μ and σ are related to $\bar{y}$ and s by eqs. (A.8) and (A.9).

If base 10 logarithms are used instead of natural logarithms, we distinguish the distribution parameters by use of primes, μ'_N and σ', and the relations become

$$\mu'_S = \mu'_N + 2\ell n(10)(\sigma')^2$$

$$\mu'_V = \mu'_N + 3\ell n(10)(\sigma')^2$$

where $\ell n(10) = 2.3026$.

The distribution of particle mass with respect to diameter is taken to be equivalent to the volume distribution with respect to diameter. This implies that all particles have the same density.

DISTRIBUTION HISTOGRAM

For computation purposes, the continuous lognormal distribution is replaced by a histogram. The computer program, via subroutine DSTBN, does this automatically by use of the distribution parameters and the number of size classes, NDSTR, which is input by the user or on default of input is set to 100.

μ_N, σ, and μ_V are determined from DMEAN and SD via

$$\mu_N = \ell n(\text{DMEAN})$$

$$\sigma = \ell n(\text{SD})$$

$$\mu_V = \mu_N + 3\sigma^2 \quad .$$

Define the normal distribution function argument x as

$$x = \frac{\ell n(\delta) - \mu_V}{\sigma}$$

where δ is particle diameter. Then

$$N(x) = \frac{1}{\sqrt{2\pi}} \int_{-\infty}^{x} \exp(-t^2/2)dt \quad .$$

Subroutine DSTBN constructs the particle size class histogram as follows. Each size class contains a constant volume fraction, ΔN_V, of

$$\Delta N_V = 1/\text{NDSTR} \quad .$$

Let D_i, i = 1,2.....,NDSTR, be the upper (i.e., the larger particle) boundary diameter of the i-th particle size class. The histogram is ordered with the largest particles in the first size class, and so on. Then, for the i-th size class

$$N(x_i) = i\Delta N_V$$

and

$$\ell n(D_{i+1}) = x_i\sigma + \mu_V \quad .$$

The upper boundary of the first size class, D_1, and the lower boundary of the last size class, $D_{NDSTR+1}$, are special cases. These are taken to be the diameters at $\Delta N_V/2$ and $1-\Delta N_V/2$, respectively. That is,

$$N(x_1) = \frac{\Delta N_V}{2}$$

and

$$N(x_{NDSTR+1}) = 1 - \frac{\Delta N_V}{2} \quad .$$

In these calculations x is determined from given N(x) via equation 26.2.23 of ref. 37.

The central particle diameter for the i-th class, δ_i, is given by

$$\delta_i = \sqrt{D_i D_{i+1}} \quad .$$

If NDSTR = 1, a single size class is created with

$$D_1 = (DMEAN) * (5.0 * SD)$$

$$D_2 = (DMEAN) / (5.0 * SD)$$

and

$$\delta_1 = DMEAN \quad .$$

APPENDIX B

POWER LAW PARTICLE SIZE DISTRIBUTION

DATA ANALYSIS

Suppose that we have a sample of fallout particles of mass m and average density ρ, and we size the sample into N fractions, the ith fraction of mass ΔF_i containing particles in the diameter range $\Delta\delta_i$ centered on δ_i. To obtain the power law distribution parameters k/m and X (sec. 2.1.6), we plot $\log_a(\Delta F_i/\Delta\delta_i)$ vs. $\log_a(\delta_i)$ where a is the logarithm base. A straight line is fitted to the plot, and we obtain for this line

$$\text{intercept} = c = \log_a\left(\frac{\pi\rho k}{6m}\right)$$

$$\text{slope} = s = 3 - X \quad .$$

Therefore, the DELFIC distribution parameters are

$$X = 3 - s$$

$$k/m = 6\, a^c/(\pi\rho)$$

where m is in kg, δ in meters and ρ in kg m^{-3}.

DISTRIBUTION HISTOGRAM

DELFIC creates a histogram representation of the power law distribution (Subroutine DISTBN) for use in the fallout calculations. The histogram consists of NDSTR particle size classes of equal mass fraction ΔF = 1/NDSTR.

Let D_i be the upper (i.e., larger particle) boundary of the i-th particle size class. The table is ordered with the largest particles in the first class, and so on. If we assume that the smallest particle in the NDSTRth class is much smaller than D_{NDSTR}, we see from Eq. (2.1.18) that

$$D_{NDSTR}^{4-X} = \frac{6(4 - X)\Delta F}{\pi\rho} \left(\frac{m}{k}\right) .$$

By recursive use of this relation with Eq. (2.1.18), we find that

$$D_i = (NDSTR - i + 1)^{\frac{1}{4-X}} D_{NDSTR} .$$

Size class central diameters, δ_i, are

$$\delta_i = \sqrt{D_i D_{i+1}} .$$

To establish a central and lower boundary diameter for the NDSTRth class, we say that

$$\delta_{NDSTR} = \left(\frac{1}{2}\right)^{\frac{1}{4-X}} D_{NDSTR}$$

and

$$D_{NDSTR+1} = (\delta_{NDSTR})^2 / D_{NDSTR} .$$

APPENDIX C

FALLOUT PATTERN COMPARISON BY THE FIGURE-OF-MERIT METHOD

Rowland and Thompson[39] developed this method for comparison of pairs of fallout contour maps by computation of a single index, the FM, that is a measure of contour overlap between them. For each contour common to the patterns, the area overlapped and the area not overlapped is calculated. The areas are weighted by the average radiation level between successive contours. Sums over all contours of weighted overlapped areas and weighted total areas are computed, and the FM is the ratio of the two sums. For completely overlapped, perfectly matched patterns, FM = 1; for no overlap, FM = 0.

Mathematically, FM is

$$FM = \frac{\sum_{i=1}^{N} \frac{(r_i + r_{i-1})}{2} (a_i - a_{i-1})}{\sum_{i=1}^{N} \frac{(r_i + r_{i-1})}{2} (A_i - A_{i-1})}$$

where

N is the number of contours in the patterns. The summations are from highest contour to lowest

r_i is activity of the i th contour (Roentgen/hr), $r_o = 10\ r_1$

a_i is common (i.e., overlapped) area for the i th contours. $a_o = 0$.

A_i is total area of the i th contour. The summation in the denominator is computed for both patterns, and the largest sum is used. $A_o = 0$.

The FM has been found to have limited utility as a measure of fallout prediction accuracy. This is mainly for two reasons. First, and most important, is that being a measure of overlap, the FM is strongly biased in favor of overprediction; that is, it favors predictions that cover a large area, and therefore overlap the observed pattern, regardless of other considerations. Second, the FM method imposes no penality for missing or extra contours; contours not common to both patterns are simply ignored.

APPENDIX D

GLOSSARY OF SYMBOLS

A	activity
c_p	specific heat of air and water vapor at constant pressure
c_{pa}	specific heat of dry air at constant pressure
c_{pw}	specific heat of water vapor at constant pressure
c_s	specific heat of soil
d	scaled depth of burst (ft $KT^{-1/3.4}$), differential operator
D	particle diameter at size class boundary
E	turbulent kinetic energy per unit mass of cloud
f	particle settling speed
F	rate of fallout from the cloud
F_T	total number of equivalent fissions
g	acceleration of gravity
H	heat energy
H_c	vertical cloud radius
H_R	relative humidity
k	Von Karman's constant (0.35)

Glossary (con't.)

k_2	cloud rise kinetic energy to turbulent energy conversion parameter (eq. (2.2.1a))
k_3	cloud turbulent energy dissipation constant (eq. (2.2.4a))
L	latent heat of vaporization of water or ice, Monin-Obukhov length
m	mass of cloud
m_s	mass of fallout
m_a	mass of air
m_w	mass of water
N_D	Davies number (eq. (2.2.9))
P	atmospheric pressure
P_{ws}	saturation water vapor pressure
q(x)	$\frac{1 + x/\varepsilon}{1 + x}$, where x is water vapor mixing ratio
Q	activity or mass in a fallout parcel
$\vec{r}$	horizontal position vector
R_a	ideal gas law constant for air

Glossary (con't.)

R_c	cloud radius
s	geometric standard deviation of particle diameter for a log-normal particle size distribution, soil mixing ratio (soil mass per unit mass of dry air), particle settling speed slip factor (eq. (2.2.11)), measurement height of surface wind speed
S	$4\pi R_c^2$
t	time
t_{2m}	time of the second fireball temperature maximum
T	temperature
T*	Tq(x), i.e., virtual temperature
Υ_j	particle deposition time from the base of the jth wind stratum
u	cloud rise velocity
u_*	air friction velocity in the atmospheric surface layer (eq. (3.3.4))
$\vec{U}$	horizontal wind vector
v	characteristic cloud rise velocity (eq. (2.2.1b))
V	cloud volume
w	condensed water mixing ratio (mass of condensed water per unit mass of dry air), vertical wind component

Glossary (con't.)

W	total energy yield of the nuclear explosion (KT)
W_F	fission yield (KT)
x	water vapor mixing ratio (water vapor mass per unit dry air mass), coordinate in the west-to-east direction
X	power-law particle size distribution exponential parameter
Y_j	fission yield of jth mass chain
z	vertical coordinate
z_o	aerodynamic surface roughness length (eq. (3.3.4))
α	wind direction angle, limiting vertical distance for wind data interpolation (eq. (3.5.2))
β	limiting horizontal distance for wind data interpolation (eq. (3.5.2)), ratio of Lagrangian to Eulerian time scales (eq. (3.3.2))
β'	ratio of gas density to total density of cloud = $\frac{1+x}{1+x+s+w}$
δ	particle diameter
δ_{50}	median particle diameter
ϵ	turbulent energy density dissipation rate
η	air viscosity

λ	scaled height of burst (ft $KT^{-1/3}$), activity decay constant
Λ	scaled height of burst (ft $KT^{-1/3.4}$)
μ	cloud entrainment parameter (eq. (2.2.5a))
ξ	ratio of molecular weights of air and water (29/18)
ρ	air density
ρ_p	particle density
σ	standard deviation, σ^2 variance
τ_o	wind shear stress in the atmospheric surface layer (eq. (3.3.3))
ϕ	fraction of available heat energy in the initial cloud used to heat air and soil
$\omega(x,y)$	contribution of activity or mass from a deposit increment of fallout at map point x,y
ω_{min}	threshold activity or mass contribution from a single fallout deposit increment at a map point

SUBSCRIPTS

a	air
B,b	cloud or fallout parcel base
e	ambient
ert	entrainment

SUBSCRIPTS (con't.)

g,GZ	ground
i	initial cloud
r	refractory mass chain
s	stabilization, soil
T,t	cloud or fallout parcel top
w	water or water vapor
$_{\parallel}$	along wind
$_{\perp}$	cross wind

DISTRIBUTION LIST

DEPARTMENT OF DEFENSE

Command & Control Technical Center
ATTN: C-312, R. Mason

Defense Advanced Rsch. Proj. Agency
ATTN: TIO

Defense Intelligence Agency
ATTN: DIO-GPF, W. Magathan
ATTN: DB-4C, P. Johnson
ATTN: RDS-3C
ATTN: DB-1, F. Walker
ATTN: DN
ATTN: Dir 4

Defense Nuclear Agency
ATTN: NATA
ATTN: RAAE
ATTN: STSP
ATTN: SPTD
ATTN: STNA
ATTN: STRA
ATTN: RAEE
ATTN: NATD
4 cy ATTN: TITL

Defense Technical Information Center
12 cy ATTN: DD

Field Command
Defense Nuclear Agency
ATTN: FCP, J. Digrazia
2 cy ATTN: FCPR

Field Command
Defense Nuclear Agency
Livermore Division
ATTN: FCPRL, L-395
ATTN: FCPRL

Field Command
Defense Nuclear Agency
Los Alamos Branch
ATTN: FCPRA

Interservice Nuclear Weapons School
ATTN: Document Control

Joint Chiefs of Staff
ATTN: SAGA/SSD
ATTN: SAGA/SFD
ATTN: J-5
ATTN: J-3

Joint Strat. Tgt. Planning Staff
ATTN: JL
ATTN: JP
ATTN: JPS
ATTN: JLTW

Undersecretary of Defense for Rsch. & Engrg.
ATTN: K. Hinman

DEPARTMENT OF THE ARMY

Deputy Chief of Staff for Rsch., Dev., & Acq.
Department of the Army
ATTN: DAMA-CSM-N

Harry Diamond Laboratories
Department of the Army
ATTN: DELHD-N-TD
ATTN: DELHD-N-P
ATTN: Chairman Nuc. Vulnerability Branch
ATTN: DELHD-I-TL
ATTN: DELHD-N-D

U.S. Army Armament Research & Development Command
ATTN: DRDAR-LCN-E

U.S. Army Ballistic Research Labs.
ATTN: DRDAR-VL
ATTN: DRDAR-TSB-S
ATTN: DRDAR-BLV

U.S. Army Command & General Staff College
ATTN: Combined Arms Research Library

U.S. Army Concepts Analysis Agency
ATTN: MOCA-WG

U.S. Army Foreign Science & Tech. Center
ATTN: DRXST-SD-1

U.S. Army Mobility Equip. R&D Command
ATTN: DRDME-RT, K. Oscar
ATTN: DRDME-WC, Technical Library, Vault

U.S. Army Nuclear & Chemical Agency
ATTN: MONA-ZB, D. Panzer
ATTN: Library

U.S. Army War College
ATTN: Library

DEPARTMENT OF THE NAVY

Center for Naval Analysis
ATTN: NAVWAG

Naval Academy
ATTN: Nimitz Library/Technical Rpts. Branch

Naval Postgraduate School
ATTN: Code 56PR
ATTN: Code 1424

Naval Research Laboratory
ATTN: Code 8440, F. Rosenthal
ATTN: Code 2627

Naval Surface Weapons Center
ATTN: Code R14
ATTN: Code U41
ATTN: Code F31
ATTN: Code U12
ATTN: Code F30

DEPARTMENT OF THE NAVY (Continued)

Naval Surface Weapons Center
ATTN: Code DG-50

Naval War College
ATTN: Code E-11, Tech. Service

Naval Weapons Evaluation Facility
ATTN: Technical Director
ATTN: G. Binns

Office of Naval Research
ATTN: Code 431
ATTN: Code 200

DEPARTMENT OF THE AIR FORCE

Assistant Chief of Staff
Studies & Analyses
Department of the Air Force
ATTN: AF/SAGF
ATTN: AF/SAMI
ATTN: H. Zwemer

Air Force Weapons Laboratory
Air Force Systems Command
ATTN: SUL
ATTN: NSSB

Ballistic Missile Office
Air Force Systems Command
ATTN: MNR, R. Landers

DEPARTMENT OF ENERGY CONTRACTORS

Lawrence Livermore National Laboratory
ATTN: L-24, G. Staehle
ATTN: L-9, R. Barker
ATTN: L-21, M. Gustavson
ATTN: L-8, F. Barrish

Los Alamos National Scientific Laboratory
ATTN: R. Sandoval
ATTN: E. Chapin
ATTN: R. Stolpe
ATTN: W. Lyons
ATTN: M/S 632, T. Dowler

Sandia National Laboratories
Livermore Laboratory
ATTN: T. Gold

Sandia National Laboratories
ATTN: J. Kaizur
ATTN: 3141

OTHER GOVERNMENT AGENCIES

Central Intelligence Agency
ATTN: OSR/SEC
ATTN: OSR/SE/F, A. Rehm
ATTN: OSI/NED

Federal Emergency Management Agency
ATTN: Hazard Eval. & Vul. Red. Div.
ATTN: Deputy Director, J. Nocita
ATTN: Asst. Dir. for Rsch., J. Buchanon

U.S. Arms Control & Disarmament Agency
ATTN: C. Thorn

DEPARTMENT OF DEFENSE CONTRACTORS

Academy for Interscience Methodology
ATTN: N. Pointer

Atmospheric Science Associates
ATTN: H. Norment

66th MI Group
ATTN: RDA for T. Greene

BDM Corp.
ATTN: J. Braddock

Decision-Science Applications, Inc.
ATTN: D. Puch

General Electric Company—TEMPO
ATTN: DASIAC

General Electric Company—TEMPO
ATTN: DASIAC

Historical Evaluation & Rsch. Org.
ATTN: T. Dupuy

Hudson Institute, Inc.
ATTN: H. Kahn
ATTN: C. Gray

JAYCOR
ATTN: E. Almquist

Kaman Sciences Corp.
ATTN: V. Cox
ATTN: F. Shelton

Kaman Sciences Corp.
ATTN: T. Long

McLean Research Center, Inc.
ATTN: W. Schilling

Mission Research Corp.
ATTN: D. Sowle

Pacific-Seirra Research Corp.
ATTN: G. Lang

R & D Associates
ATTN: R. Montgomery
ATTN: C. MacDonald
ATTN: P. Haas

Rand Corp.
ATTN: Library
ATTN: T. Parker
ATTN: J. Digby

Santa Fe Corp.
ATTN: D. Paolucci
ATTN: N. Polmar
ATTN: E. Ortlieb
ATTN: M. Wade
3 cy ATTN: A. Billones

DEPARTMENT OF DEFENSE CONTRACTORS (Continued)

Science Applications, Inc.
ATTN: M. Drake
ATTN: J. Martin
ATTN: C. Whittenbury

Science Applications, Inc.
ATTN: J. Goldstein
ATTN: J. McGahan
ATTN: W. Layson

DEPARTMENT OF DEFENSE CONTRACTORS (Continued)

System Planning Corp.
ATTN: F. Adelman
ATTN: J. Douglas
ATTN: G. Parks